Applied Catalysis B: Environmental 237 (2018) 1044–1058

Contents lists available at ScienceDirect

Applied Catalysis B: Environmental

journal homepage: www.elsevier.com/locate/apcatb

Preferential oxidation of CO in $H_2/H_2O/CO_2$ water–gas shift feedstocks over Cu-based carbon nanotubes-supported heterogeneous catalysts

Venkata D.B.C. Dasireddy*, Blaž Likozar, Jignesh Valand[1]

Department of Catalysis and Chemical Reaction Engineering, National Institute of Chemistry, Hajdrihova 19, 1001 Ljubljana, Slovenia

ARTICLE INFO

Keywords:
Selective oxidation reaction
Carbon monoxide conversion
Carbon dioxide co-feeding
Non-noble metal catalysis
Hydrogen purification and fuel cells

ABSTRACT

Selective carbon monoxide (CO) oxidation reaction was studied over mono- and bimetallic Co, Cu and Fe, as well as Cu–Co and Cu–Fe heterogeneous catalysts, using multi-walled carbon nanotubes (MWCNT) as substrates. Materials were synthesized by wet (co-)impregnation technique and characterised. It was found that hydrophilic hydroxyl and carboxyl nanotubes' (CNT) functional groups were favourable for a strong metal–support interaction. The catalytic conversion performance for preferential CO oxidation (PROX) process was carried out in hydrogen, water, and carbon dioxide-containing feedstock gasses. The addition of iron or cobalt to Cu/CNT improved the activity with comparison to Cu/CNT. The optimized Cu–Fe/CNT could preferentially oxidize dilute CO in H_2-rich simulated WGS streams within a wide temperature range of 120–220 °C. The temperatures, where 50% CO conversion was achieved, were as follows: Cu–Fe/CNT (120 °C) > Cu–Co/CNT (140 °C) ≈ Cu/CNT (140 °C). A high determined selectivity towards CO_2 for Cu–Fe/CNT could be attributed to the presence of $CuFe_2O_4$ and the synergy between Co and Cu for Cu-Co/CNT. At 220 °C and in a 1% CO/1% O_2/10% H_2O/10% CO_2/60% H_2/18% He stream, Cu–Fe/CNT could achieve a 100% CO conversion, granting a low H_2 conversions, not differing from those in the absence of CO_2, while its turnover performance remained stable for a longer continuous time-on-stream with basically no deactivation. By comparison, Cu–Fe/CNT exhibited a higher apparent rate and lower activation energy of CO conversion (with and without H_2O and CO_2).

1. Introduction

Hydrogen-fuelled polymer electrolyte membrane (H_2-PEM) fuel cells have been applied in the electric vehicles from the viewpoint of an increased renewable energy usage efficacy and a significantly lowered carbon oxide emissions [1]. Still, a challenge for developers exists to overcome the difficulties with the supply and storage of hydrogen for H_2-PEM fuel cells, to be used in various mobile applications [2]. For H_2-PEM, hydrogen should be produced onboard in a fuel-processing unit by reforming or by partially oxidizing liquid fuels, such as liquefied petroleum gas (LPG), gasoline or methanol, and then further processed by a water–gas shift catalyst to maximize the yield of hydrogen [3]. Thus, an H_2-rich feed to H_2-PEM, still polluted with carbon-containing residuals, *e.g.* 1 mol. % CO can induce a poisoning of H_2-PEM cell platinum anode catalyst due to a durable adsorption of CO to platinum which subsequently decreases productivity [4]. Therefore, CO concentration has to be reduced to a tolerable level. Among the various methods for removing CO from H_2-rich feed gas, the selective oxidation of CO has been recognized as a cost effective one to reduce the CO concentration down to 10 ppm or less, which is necessary for the operation of a fuel cell with a minimal loss of hydrogen [5]. However, hydrogen oxidation competes with the one of CO leading to a decrease of hydrogen fuel efficiency. In order to reduce CO to the desired level and to minimize H_2 consumption, selective and active catalysts are needed. A proper material for CO PROX reaction should have a high activity, selectivity, and stability from 80 to 220 °C [6].

A number of catalysts have been investigated for CO PROX reaction. In recent years, there has been a great interest in the CO oxidation reaction over gold-based catalysts due to two main reasons; *i.e.* they exhibit an extraordinarily high activity in a low-temperature range, which is appropriate for fuel cell applications, and the rate of CO oxidation exceeds that of hydrogen in a comparable temperature range [7,8]. The gold catalysts, supported on reducible transition metal oxides such as Fe_2O_3, exhibit a considerably improved activity for CO oxidation, which is attributed to their ability to deliver reactive oxygen [7]. The gold catalysts with inert support materials such as Al_2O_3, MgO or SiO_2 are intrinsically less active [8]. For gold-based catalysts, various authors [9–11] agree that the factors, controlling activity and

* Corresponding author. Tel.: +386 1 4760 224; fax: +386 1 4760 300.
E-mail address: dasireddy@ki.si (V.D.B.C. Dasireddy).
[1] Present address: Department of Materials Science, Sardar Patel University, Vallabh Vidyanagar-388120, Gujarat, India.

https://doi.org/10.1016/j.apcatb.2018.06.069
Received 25 April 2018; Received in revised form 22 June 2018; Accepted 26 June 2018
Available online 28 June 2018
0926-3373/

selectivity, are metal particle sizes, SMSI (strong metal–support interaction) and the choice of support. Other effective materials include supported Pd, Pt, Rh, Ru and modified Cu catalysts [12]. For the selectivity of CO *versus* H_2 oxidation reaction, the effect of a support on activity has also been investigated on Pt catalysts, exhibiting quite a reaction determining the role, whereas activity trend followed the order of zeolite A > mordenite > zeolite X > alumina [13].

While neat CO oxidation is a well-studied reaction, the selective oxidation of CO in H_2-, H_2O- and CO_2-rich streams is not nearly as well studied in the literature [12,14,15]. Due to CO, CO_2, H_2, and H_2O all often being present together, also owing to the water–gas shift reaction, it is important to study the selective CO oxidation within a realistic gas mixture [16]. In addition to a high activity and selectivity, a suitable PROX catalyst thus has to be stable under a high quantity of H_2O and CO_2, present in reformate stream [13,17]. In general, both H_2O and CO_2 reduce CO conversion and diminish catalyst activity, especially at low temperatures; nonetheless, a good WGS catalyst can withstand this decrease with a high amount of H_2O being present [13,18]. The ability of a catalyst to allow for a wide range of CO_2 concentrations in PROX generally depends on its composition and support nature (acid supports are thus more resistant to deactivation). It was recently reported by Tabakova et al [19]. that gold supported on Ce–Fe composite system can effectively bear a high amount of H_2O and CO_2 with a good performance in CO PROX reaction. In general, reformate of the WGS reaction contains approximately 10–20 mol. % H_2O vapor and 15–25 mol. % CO_2 [12,14,15]. Avgouropoulos and co-workers [19,20] investigated the effect of H_2O and CO_2 on CO PROX reaction and observed a negative effect of H_2O and CO_2 on the performance of no-precious metal Cu–Ce catalyst, and that temperature higher than 200 °C is required for a sufficient CO conversion. Thus, an emerging catalyst with a high CO PROX activity and the resistance to the presence of H_2O and CO_2 is one of the primary general research interests.

From the past decade, CNT as a support has attracted an enormous interest owing to their superior and unique optical, electronic and mechanical properties [21,22]. With the evolution of this field, catalysts containing metal oxides and CNT have been fabricated by various approaches due to their promising application for solar cells, electrochemical energy storage materials and active catalysts [23]. It has been described that the oxygen-containing functional groups, specifically, the phenolic hydroxyl and carboxyl on the surface of CNT, are beneficial to granting a strong interaction between metal and CNT and obtaining highly-dispersed metal particles, which can promote the activity of metal-supported CNT [22,23]. Thus, carbon nanotubes can be a functional material as a catalyst support, and therefore, the investigations of effectively impregnating a metal/metal oxide onto the surface of CNT is of an utmost importance, particularly when designing a material for a specific catalytic reaction.

Recently, an enhanced performance of CO PROX has been preliminarily reported over Ru/CNT catalysts [23]. Furthermore, carbon nanotube-supported Pt–Co bimetallic catalysts (Pt–Co/CNT) were synthesized for the preferential oxidation of CO in an H_2-rich stream [24]. These results indicated that the addition of Co on to Pt/CNT catalysts significantly improved the performance, making CNT superior to other carriers assessed, supporting the same composition of Pt–Co. In addition to the effect of support, the synergistic interaction between Pt metal surface and CoO was largely responsible for a notable CO PROX performance of these materials. Furthermore, Cu_xO–CeO_2/CNT catalysts also exhibited a high catalytic activity with the temperature window of total CO conversion ranging from 135 to 175 °C [22].

Taking into account these premises, the current study compares the catalytic behaviour of Co, Cu and Fe nanoparticles supported on high-purity CNT. The effect of transition metal itself, the surface chemistry of carbon support, and the effect of the Co and Fe addition to Cu-containing materials are assessed for the preferential CO oxidation reaction under hydrogen-rich conditions. CNT-supported catalysts are evaluated in the temperature range from the ambient- to the conventional operational range of the low-temperature (LT) WGS units (~200 °C). A special attention is paid to obtaining the catalysts with a high activity and selectivity towards the CO_2 formation (H_2 oxidation to H_2O should be avoided) at the typical operating temperature of the LT H_2-PEM FC (~100 °C) in onboard fuel processors. Also, unlike many previous works, the impact in this investigation is also placed on the effect of H_2O and CO_2 on CNT catalysts, while their stability is also tested in longer-duration process experiments.

2. Experimental

2.1. Heterogeneous catalyst preparation

2.1.1. Functionalization of commercial carbon nanotubes

CNT, measuring 10–30 nm in diameter and 5–15 mm in length were purchased from Sigma–Aldrich (CAS Number: 308068-56-6). The functionalization of carbon nanotubes was performed by following the method, outlined by Gao et al. [25]. Commercial CNT was consequently dispersed in ethanol, and ultrasound was applied to the solution for 30 min to separate them and improve the contact between nanotube surface and oxidant molecules. The mixture was then heated from the ambient temperature to 120 °C for 60 min and cooled back. The dispersion was subsequently sonicated again for 30 min, washed extensively with distilled water and filtered under vacuum (to removing all liquid). The layer, deposited on the filter, was washed with deionised water until the pH of the filtered solution was about 6–7. The product was finally dried at 80 °C in an oven (to the equilibrium dryness) and kept in a desiccator for further use.

2.1.2. Synthesis of Cu, Fe and Co nanocomposites supported on commercial carbon nanotubes

Catalysts, containing 10 wt. % of metals (Co, Cu and Fe) and supported on CNT, were prepared by wet impregnation methods. Typically, the calculated quantities of metal nitrates (Analytical grade; Sigma–Aldrich) were dissolved in 100 mL of deionized water. This solution was consequently dropwise (1 h) added to functionalised carbon nanotubes, dispersed in 100 mL of deionized water, which was performed under a steady stirring (500 rpm). This mixture was further stirred for 4 h at the temperature of 80 °C. The paste obtained was then dried overnight (16 h) at 90 °C and subjected to the calcination at 300 °C for 4 h under the airflow of 100 mL min^{-1}. Prepared catalysts were denoted as Co/CNT, Cu/CNT, and Fe/CNT.

2.1.3. Synthesis of Cu–Co or Cu–Fe nanocomposites supported on commercial carbon nanotubes

Bimetallic catalysts, containing 10 wt. % Cu–5 wt. % Fe or 10 wt. % Cu–5 wt. % Co and supported on CNT were prepared by co-impregnation methods. Typically, the calculated quantities of metal nitrates (Analytical grade; Sigma–Aldrich) were dissolved in 100 mL of deionized water. This solution was consequently dropwise (1 h) added to functionalised carbon nanotubes, dispersed in 100 mL of deionized water, which was performed under a steady stirring (500 rpm). The paste obtained was then dried overnight (16 h) at 90 °C and subjected to the calcination at 300 °C for 4 h under 100 mL min^{-1} of air. 10 wt. % Cu–5 wt. % Co and 10 wt. % Cu–5 wt. % Fe catalysts were denoted as Cu–Co/CNT and Cu–Fe/CNT.

2.2. Heterogeneous catalyst characterisation

Physisorption analyses were carried out by firstly degassing the catalysts in the N_2 atmosphere for 4 h at 200 °C. The degassed samples were examined in the Micrometrics ASAP 2020. H_2, O_2, CO, CO_2 and NH_3 chemisorption analyses were performed using the Micromeritics 2920 Autochem II Chemisorption Analyser. Prior to chemisorption examination, temperature-programmed reduction (TPR) was carried out on catalyst samples utilizing the same instrument. Before the reduction

of a sample in TPR, catalysts were pretreated by heating under the stream of argon (30 mL min^{-1}) at 400 °C for 30 min, and consequently cooling back to 80 °C. Thereafter, 4.9 mol. % hydrogen in argon was used as the reducing agent at the flow rate of 30 mL min^{-1}. Samples were analysed from the ambient temperature (25 °C) to 950 °C using the ramp rate of 10 °C min^{-1}. Following reduction, catalysts were pretreated under the stream of helium (30 mL min^{-1}) at 350 °C for 60 min. Temperature was subsequently linearly (10 °C min^{-1}) decreased to 80 °C A selected gas (4.9 mol. % H_2 in Ar / 5 mol. % O_2 in Ar / 10 mol. % CO in He / 10 mol. % CO_2 in He) was then passed over the catalysts at the flow rate of 30 mL min^{-1} for 60 min. Excess gas was consequently removed by purging with helium for 30 min (30 mL min^{-1}). The temperature was then again raised gradually to 600 °C by ramping at 10 °C min^{-1} under the flow of helium and the desorption data of H_2, O_2, CO, CO_2 and NH_3 was recorded separately.

The dispersion of the metals on CNT was calculated using CO chemisorption data, assuming the metal/CO chemisorption ratio of 1 [26,27]. Powder X-ray diffraction (XRD) studies were conducted using the PANalytical X'Pert Pro. The scans from 10 to 90° were carried out using the CuKα radiation source the wavelength of 1.5406 Å. Particle size, morphology, and elemental mapping, performed by energy-dispersive X-ray spectroscopy (EDXS) analysis, were further investigated using the Cs-corrected scanning transmission electron microscope (TEM) (JEOL, JEM-ARM200CF), equipped with JEOL EDXS system.

Operando Diffuse Reflectance Infrared Fourier Transform (DRIFT) spectra were recorded in the range of 900–4000 cm^{-1} using an infrared analyser (Perkin Elmer; Frontier) equipped with mercury cadmium telluride detector. The high-temperature reaction chamber (PIKE Technologies, DiffusIR) was used in order to monitor the catalyst surface under reaction conditions. Experiments were conducted using 10 mg of sample placed into a sample holder made from sintered ceramics (5 mm internal diameter) and finely smoothed to create a flat surface. Prior to analyses, catalysts were activated *in situ* in 20 mL min^{-1} He flow at 250 °C for 1 h. Consequently, a gaseous 10 mol. % CO in He (20 mL min^{-1}) was flown through the catalysts for 15 min, and hence the employed gas was switched back to He. The same procedure was repeated at each temperature, whereas spectra were recorded from 30 °C to 200 °C. Spectra were collected with the resolution of 4 cm^{-1}, attaining 32 scans for averaging.

Thermo-gravimetric analysis (TGA) and differential scanning calorimetry (DSC) was performed for catalyst samples (9–10 mg), contained in an alumina crucible under the flow of air (30 mL min^{-1}), using Thermal Analyser SDT Q600 instrument. Temperature was increased from the ambient temperature (25 °C) to 1000 °C at the heating rate of 10 K min^{-1}. Raman spectra were recorded at the ambient temperature (25 °C) with the green laser wavelength of 532 nm using WITec alpha300 RAS instrument.

Transmission electron microscopy (TEM), scanning transmission electron microscopy (STEM) and electron energy loss spectroscopy (EELS) were performed on Jeol ARM 200 CF atomic resolution STEM with probe Cs corrector. For chemical analysis, Dual EELS Quantum ER system from Gatan and Jeol Centrino EDXS system with 100 mm^2 solid-state detectors were used. For TEM sample preparation powder samples were mixed with ethanol anda drop of suspension was placed on lacy carbon-coated Ni grids. The x-ray photoelectron spectroscopy (XPS or ESCA) analyses were carried out on the PHI-TFA XPS spectrometer produced by Physical Electronics Inc. Samples were placed on a sample holder and introduced in an ultra-high vacuum spectrometer. The analyzed area was 0.4 mm in diameter and the analyzed depth of about 3–5 nm; this high surface sensitivity is a general characteristic of the XPS method. Sample surfaces were excited by X-ray radiation from monochromatic Al source at the photon energy of 1486.6 eV. The high-energy resolution spectra were acquired by the energy analyzer operating at the resolution of approximately 0.6 eV and pass energy of 29 eV. During data processing, the spectra from the surface were aligned by setting the C 1 s peak at 285.0 eV, characteristic for C—C bonds. The accuracy of binding energies was approximately ± 0.1 eV. Quantification of surface composition was performed from XPS peak intensities taking into account relative sensitivity factors provided by the instrument manufacturer.

2.3. Heterogeneous catalyst performance

CO PROX catalytic experiments using the synthesized materials were carried out in a vertical fixed-bed U-shaped quartz reactor (100 cm length and 1.5 cm internal diameter). The electric furnace, fitted with a temperature-programmed controller, heated the reactor, and the temperature of the reactor was continuously monitored using a type K thermocouple. The flow rates of gases were measured and controlled by the Brooks mass flow controllers. Prior to reactions, each catalyst (volume of 1 mL and mass in the range of 0.3-0.4 g) was pretreated *in situ* in the flow of He (50 mL min^{-1}) at 400 °C for 1 h. Reactions were consequently performed at different temperatures from 40 to 220 °C, using the steps of 20 °C. Feed composition typically consisted of 1 vol. % CO, 1 vol. % O_2, 60 vol. % H_2 and He as the balance (total flow rates in the range of 500 mL to 1000 mL) with gas hourly space velocity (GHSV) varying from 30,000 to 60,000 h^{-1}. In all the catalytic tests, $\lambda = 2$ was used, because this value was optimal for preferential oxidation of CO [12–15, 17, 19. 24]. To study the effect of H_2O and CO_2 on catalyst activity and selectivity, 10 mol. % of either/each compound was added in the feedstock. Outlet gases, including CO, O_2, H_2O, CO_2 and H_2 were analysed by online quadrupole mass spectrometry (MS). The signals of MS were calibrated using the mixtures with different mole fractions of CO, O_2, H_2O, CO_2 and H_2 that is, in order to determine the mole composition of the gases in the outflow. All catalytic tests were carried out in duplicate and the values, obtained for CO conversion, exhibited the standard deviation below 2%. Conversions and CO_2 selectivity were calculated from the mole fraction of products in exit stream according to the following equations [28].

$$\text{CO conversion}\,(/) = X_{CO} = (n_{CO,in} - n_{CO,out})/n_{CO,in} \quad (1)$$

$$O_2\ \text{conversion}\,(/) = X_{O_2} = (n_{O_2,in} - n_{O_2,out})/n_{O_2,in} \quad (2)$$

$$H_2\ \text{conversion}\,(/) = X_{H_2} = (2(n_{O_2,in} - n_{O_2,out}) - (n_{CO,in} - n_{CO,out}))/n_{H_2,in} \quad (3)$$

$$CO_2\ \text{selectivity}\,(/) = S_{CO_2} = (n_{CO,in} - n_{CO,out})/(2(n_{O_2,in} - n_{O_2,out})) \quad (4)$$

The apparent activity for CO oxidation was applied to compare the performance of catalysts. The activity towards the reactions of CO was expressed as the amount of the CO converted *per* mass of a catalyst *per* second, which was calculated by the following equation.

$$\text{CO activity}\,(\text{kmol}_{CO}\,s^{-1}\,kg_{cat.}^{-1}) = A_{CO} = (p\,Q_{in}\,x_{CO,in}\,X_{CO})/(R\,T\,W) \quad (5)$$

p represents the atmospheric pressure (1 bar), Q_{in} input volumetric flow rate ($m^3\ s^{-1}$), $x_{CO,in}$ input CO fraction (1 mol. %), R the gas constant (8.3145×10^3 J K^{-1} $kmol^{-1}$), T temperature (K), and W catalyst weight ($kg_{cat.}$). Apparent activation energies (E_a) were determined from reaction rate constants using the Arrhenius equation, assuming differential reactor operation ($X_{CO} \leq 10\%$) and a second order reaction (CO and O_2 effect) to be the rate-determining step.

3. Results and discussion

3.1. Heterogeneous catalyst characterisation

In the X-ray diffraction analysis of the prepared catalysts, a broad peak was observed at 26° in all material samples, corresponding to the (002) crystal plane of the CNT with a hexagonal graphite structure (Fig. 1). For all copper-containing catalysts, signals were present at a 35°, 48° and 61° on account of (111), (202) and (113) diffractions of monocrystalline copper oxide, respectively (ICDD; PDF Card 48-1548). For Fe/CNT material, there was an occurrence of iron oxide in the form

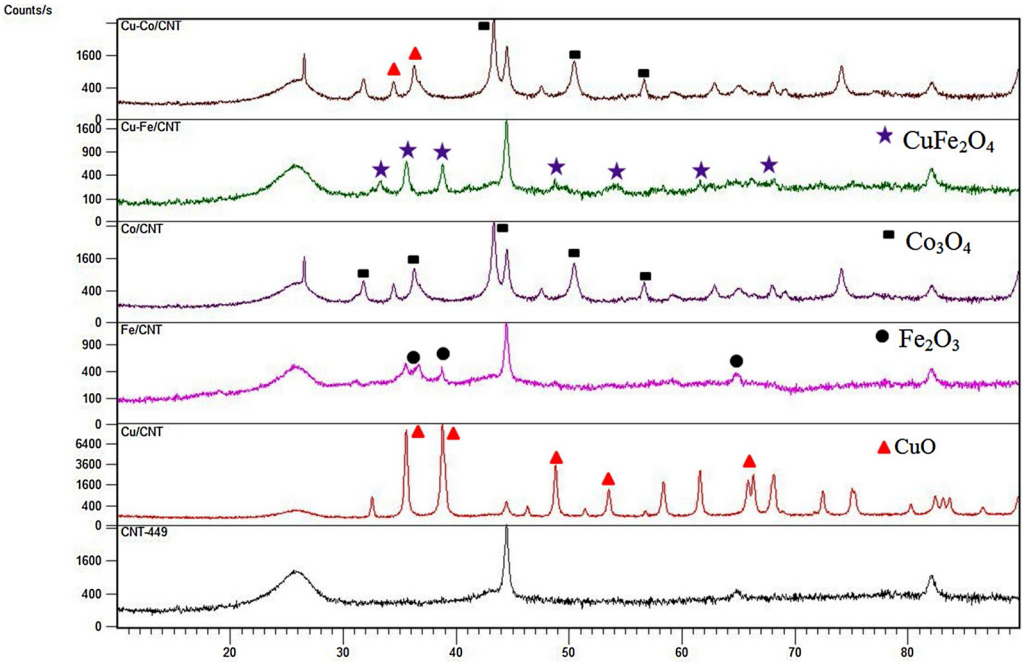

Fig. 1. Powder XRD patterns of prepared catalysts.

of α-Fe_2O_3 (ICDD; PDF Card 39-1346), peaks were observed at the 2θ of 36°, 39° and 65°. Furthermore, for Co/CNT catalysts, the signals at the 2θ of 37°, 45° and 65° indicated the presence of Co_3O_4 spinel phase (ICDD; PDF Card 42-1467). For both Co/CNT and Fe/CNT materials, the characteristic peaks of CNT were observed with a high relative intensity upon comparing it to the ones of either Co or Fe metal oxides, which indicated that these oxides were mostly in an amorphous phase, as opposed to Cu catalysts.

For Cu–Fe/CNT catalyst, in addition to CuO and Fe_2O_3 peaks, further diffraction signals were observed at the 2θ of 36°, 43° and 53° and were ascribed to (220), (311), (422) and (440) planes, respectively, namely, the characteristic diffractions of cubic $CuFe_2O_4$ phase (ICDD; PDF Card 77-0010). For Cu–Co/CNT catalysts, there were no additional peaks when compared to CuO and Co_3O_4 spinel phases (Fig. 1). In all the materials, the presence of a characteristic CNT signal, observed at 26°, indicated that the introduction of metal oxides did not affect the shells of CNT. The average crystallite sizes of oxides, which were determined by using the Scherrer equation, were in the range of 10–20 nm for all catalysts. This was in agreement with the results, obtained *via* CO chemisorption (ensuing discussion).

The textural characteristics of CNT-supported catalysts are shown in Table 1. It can be seen that the presence of a metal oxide on CNT resulted in an obvious decrease of surface area and pore volume. This decrease could be attributed to the high dispersion of metal oxides on CNT support, which blocks the micro- and mesopores of the CNT support. This drop could be. The surface oxygen-containing groups on CNT support, including carboxylic, carbonyl and hydroxyl moieties, are generally considered as initially indispensable in enhancing the hydrophilicity of CNT substrate [29,30]. In addition, these substituents can serve as the specific anchoring sites for the deposition of metal oxide species, thereby facilitating their high dispersions on the interfaces of CNT. On the other hand, calcination following impregnation may lead to the aggregation of oxide nanoparticles, even if they are anchored on the surface of CNT. Possibly, most of the deposited metal oxides did presently not form nanoparticles, while they were highly dispersed on the nanotube support in monolayer level. The actual content of Cu, Co and Fe is very near to the nominal content of the catalysts (Electronic supplementary information, Table S1). There is no drastic decrease in the metal content even after a long term stability tests of the catalysts.

Table 1
Particulate properties of prepared catalysts.

Catalyst	Surface area ($m^2\ g^{-1}$)	Pore volume ($cm^3\ g^{-1}$)	Crystallite size (nm)[a]	Metal dispersion (%)[b]
CNT	275	1.94	–	–
Cu/CNT	231	1.84	17	18.3
Co/CNT	204	1.11	12	9.3
Fe/CNT	220	1.22	10	12.2
Cu–Fe/CNT	182	0.85	14	26.3
Cu–Co/CNT	191	0.91	15	21.2

[c]Calculated using the Scherrer equation; [b] metal dispersion was defined as amount of active metal present on the surface of the catalyst which is calculated from CO Chemisorption.

The N_2 adsorption and desorption isotherms of support and all catalysts (Electronic supplementary information, Fig. S1) could be classified as type IV, and these are typical for mesoporous materials [29,31] The investigated catalysts exhibited the H1-type hysteresis loop, which is usually associated with porous materials having well-defined cylinder-like pore channels or uniform sphere agglomerates [32]. However, The N_2 physisorption isotherms and average pore diameters remained substantially the same after the metal oxide loading which indicates that the metal oxides did not disturb the pore structure of CNT but may introduce the defects to the CNT. The observed decrease of the BET surface area upon incorporation of metal oxides (Table1) is relatively low and may be mainly due to the increase of the density. For the used catalysts (Electronic supplementary information, Table S2), there appeared to be a minor decrease in the surface area and pore volume of the used catalyst in some cases. This could be attributed to the clogging of pores with the hydrocarbon molecules during the course of the reaction. For the used catalysts, XRD patterns (Electronic supplementary information, Fig. S2) showed no phase changes. There was minimal change in the structure and morphology of the used catalysts.

The TPR profile of the prepared catalysts is presented in Fig. 2. In the H_2 TPR responses of the materials, containing copper, it can be seen that there is two reduction peak groups, originating from Cu moieties; specifically, at low (below 250 °C) and high (above 250 °C) relative

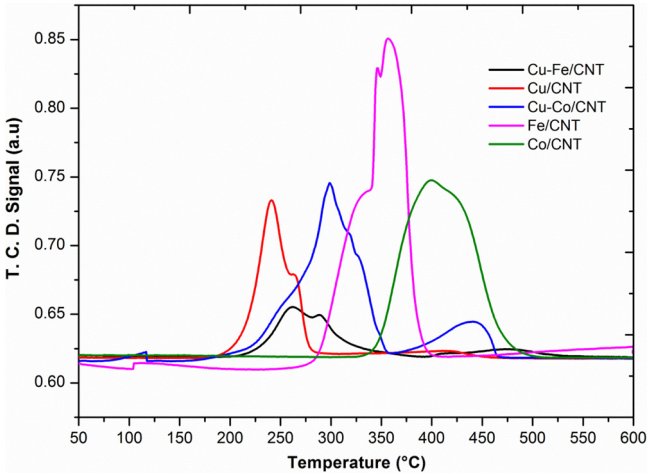

Fig. 2. TPR profile of the prepared catalysts.

temperatures [33]. For Cu/CNT catalysts, the two overlapping signals could be attributed to the reduction of agglomerated (< 250 °C) and highly dispersed (> 250 °C) CuO, respectively [34]. The first peak (230 °C) could be assigned to the reduction of monocrystalline (monolayer) Cu(II) phase, as shown in XRD (Fig. 1). Moreover, it was considered that the advent of easily (low-temperature)-reducible Cu oxide species played a key role in shifting the TPR signals of cobalt and iron to lower temperatures [35]. For Cu–Co/CNT, this occurred for a portion of Co moieties only, while some remained predominantly unreduced until approximately 440 °C. In the TPR profile of Cu–Fe/CNT catalysts, one main peak with a shoulder appeared at the transition from the noted low-temperature region, corresponding to the transition of CuO to Cu, Fe_2O_3 to Fe_3O_4 and the overlapped $CuFe_2O_4$ to Cu (directly) and Fe_2O_3, respectively [36].

The reduction of Fe/CNT occurred at a much higher temperature when compared to Cu–Fe/CNT, and a broad peak, detected in the high-temperature region for Fe/CNT, was attributed to Fe_2O_3 reduction [37]. In the TPR profile of Co/CNT catalysts, signals were observed in the range of 320–500 °C. A broad signal, observed for the transformation of Co_3O_4, could be attributed to the amorphous and well-dispersed cobalt oxide on the surface of CNT, which was also evidenced by XRD (Fig. 1). Typically, bulk Co_3O_4 exhibits a single- or two-step reduction peak in the low-temperature region of 250–400 °C [38]. It has been reported that the reduction temperature of Co_3O_4, supported on CNT, is higher than that of bulk Co_3O_4, predominantly exhibiting the transformation of Co^{3+} to Co^{2+} at 400 °C [39]. The shift in the reduction peak could thus be attributed to catalyst metal–support interaction. Even though the reduction of cobalt oxides was hindered due to the strong interaction between Co species and CNT support, the introduction of copper to cobalt decreased the reduction temperature of particular cobalt moieties. The minor peak at 450 °C for Cu–Co/CNT catalysts, therefore, corresponded to the transformation of Co_3O_4, which had not interacted with copper species. For Cu–Co/CNT, the transformation of Cu-interacting oxides was strongly influenced by the presence of copper, the reduction of Co^{3+} occurring below 350 °C in the CuO reduction range (Fig. 2).

In literature, it has been reported that the Cu^{2+} and Fe^{3+} species in mixed metal oxides were notably more difficult to be reduced than that in plain CuO or Fe_2O_3 [36]. In comparison to the transition peaks of monometallic copper, it could be found that the reduction of copper in the presence of iron and cobalt occurred at higher temperatures. In general [33,40], it is established that the smaller size of copper particles shift their reduction to lower temperatures. In addition to this, the presence of secondary metal (*i.e.* Co or Fe) inhibits the low-temperature reduction of Cu species. This could be due to the strong interaction of copper with both Co or Fe and CNT support. It could furthermore be considered that a smaller crystallite size may increase the surface density of a metal and strengthen the interaction of the metal to support [38], rendering Cu reduction more cumbersome in the case of Cu–Co/CNT and Cu–Fe/CNT catalysts in comparison to Cu/CNT. Recently, H. Yan et al [41] showed that, the Fe addition largely improves the dispersion of Cu°, which results in better reducibility because of the pronounced Cu-Fe interaction, which is also in agreement with the results observed in the present study.

CO temperature-programmed desorption (TPD) was applied for the determination and quantification of chemically-bonded oxygen species, present on the surface of carbon nanotube materials and metal oxides. [25,42,43]. The amount of CO, desorbed from supported catalysts, was higher when compared to neat CNT substrate. Thus, in the present case, the quantity of CO evolved was mainly influenced by the presence of metals upon paralleling the latter to the nature of CNT themselves (Table 2). Furthermore, chemisorption is one of the most conventional methods for characterizing the global characteristics of catalysts. The amount of gas, desorbed at a given temperature, is taken as a measure of active sites' concentration, whereas the temperature range, in which most of the process occurs, indicates their distribution. Among all investigated catalysts, bimetallic ones, supported on CNT, exhibited a high capacity of chemisorption when compared to their monometallic analogs. This could be due to the synergistic effect between Cu/Co and Cu/Fe, which increased the metal active site available on the surface of CNT. When compared to the chemisorption of H_2, the desorbed amount of CO and CO_2 was in average lower for all catalysts. Binding capacity ratios H_2/CO and H_2/O_2 are predominantly lower and higher for Cu–Fe/CNT catalyst when paralleled to monometallic materials, respectively, which indicates that this catalyst might show a good activity for CO as opposed to H_2 oxidation (Table 2).

Among monometallic catalysts, Cu/CNT material exhibited a high H_2/O_2 chemisorption ratio, which indicated that it might possess a good activity in terms of CO conversion selectivity. Furthermore, the literature on bimetallic catalytic materials discusses that the generation of an active site occurs when an oxide is deposited onto another to in turn form a surface-phase oxide [33,44]. On the respective surface of the oxides of low-oxidation state metals, metal-to-cation bond (*e.g.* Cu—Fe) exhibits a highly ionic character, and thus, when this surface is crisp, unsaturated metal cations are able to act as active sites. The strength of these surface active sites depends on the ionic character of metal-to-cation oxygen bond (*e.g.* Cu—O—Fe—O), the ratio between the charge of a cation and its ionic radius, as well as its coordination [45].

Table 2
Particulate properties of prepared catalysts.

Catalyst	H_2 chemisorbed (μmol H_2 g^{-1})	O_2 chemisorbed (μmol O_2 g^{-1})	CO chemisorbed (μmol CO g^{-1})	CO_2 chemisorbed (μmol CO_2 g^{-1})
CNT	0.08	0.12	0.02	0.08
Cu/CNT	0.57	0.68	0.22	0.42
Co/CNT	0.24	0.35	0.09	0.28
Fe/CNT	0.32	0.41	0.14	0.31
Cu–Co/CNT	0.71	0.81	0.35	0.49
Cu–Fe/CNT	0.79	0.95	0.38	0.52

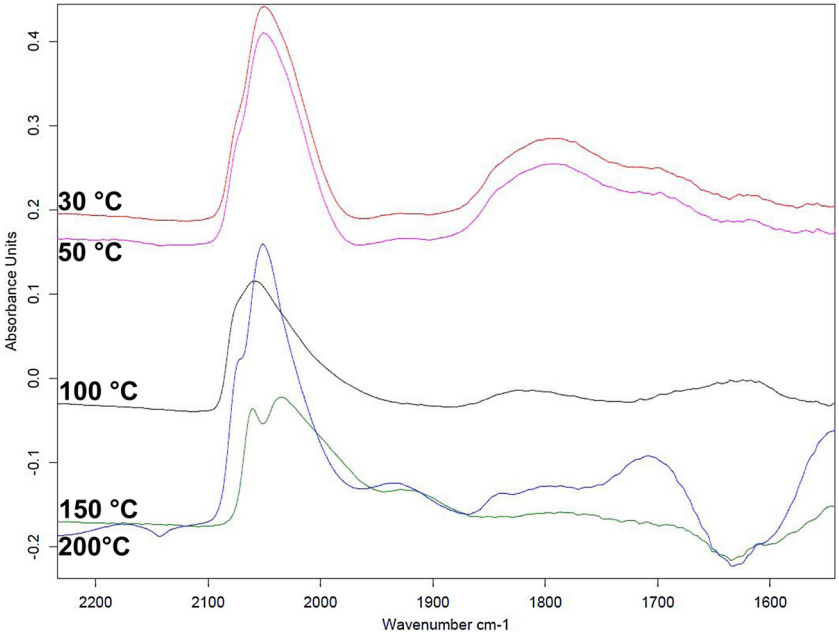

Fig. 3. DRIFT spectra of Cu–Fe/CNT catalyst.

The same mentioned sites were observed in the present study; that is, H_2/CO and H_2/O_2 ratios were predominantly lower and higher for Cu–Fe/CNT catalyst when compared to neat CNT and monometallic Cu or Fe, supported on CNT (Table 2). In bimetallic mixed oxides, a simpler situation is represented by the case, in which only two types of cations are present. When the two differ in oxidation states and electronegativity (for example Cu and Fe), the properties of one of the two components often dominate the global active site characteristics for chemisorption [46,47]. Thus, in the present case, the absorbing character of the catalysts was strongly pronounced by the presence of copper when compared to iron. The chemisorption site distributions on the surface of the materials were also strongly influenced by the nature of the support as well (Table 2), the latter acting both directly and indirectly.

Fig. 3 depicts the DRIFT spectra of Cu–Fe/CNT catalyst. Its spectrum exhibited two broad signals and a shoulder in between 1900 and 2100 cm^{-1}, suggesting a wide distribution range of adsorption sites. The shoulder peak at 2070 cm^{-1} likely corresponds to sub-carbonyl Cu $(CO)_x$ or Fe$(CO)_x$ (x = 2 or 3) species [48]. Furthermore, the signal presumably involved additional linear Cu—CO and Fe—CO moieties as well that were reported to exhibit the responses around 2030 cm^{-1} or within 2030–2070 cm^{-1} [45–47]. The main high-energy signal was assigned to CO, weakly bonded to copper and iron sites, featuring a highly-disordered structure (compared to a crystalline lattice) with a different number of nearest neighboring Cu and Fe atoms [49], which were denoted as the amorphous Cu–Fe sites on carbon nanotubes. The peak at 1960 cm^{-1}, pronounced at high temperatures, could be assigned to (linear) CO_x species, adsorbed/coordinated to semi-crystalline $CuFe_2O_4$ moieties, and crystalline copper or iron sites [49]. The linear Cu—CO and Fe—CO signal, corresponding to the same catalyst phases, shifted from 2070 cm^{-1} to 2040 cm^{-1} and rose upon temperature increase, which is likely the result of sub-carbonyl compound destabilization, making these components more visible. Carbonyl bond peak moved from 1960 cm^{-1} to 1800 cm^{-1} when the temperature was varied to between 100 °C and 200 °C (Fig. 3). The smaller response shift of linear Cu—CO and Fe—CO, compared to carbonyl bond signal, suggesting that the latter species were, by comparison, more strongly coordinated to the surface of Cu–Fe/CNT catalyst.

In the ambient temperature spectrum within the wavenumber region below 1700 cm^{-1}, signals appeared at 1600 cm^{-1} and below; these were assigned to the vibrational modes of adsorbed carbonate species [50], likely formed through the interaction of CO with CNT. Moreover, the mentioned peak at 2060 cm^{-1} (at 30–50 °C) compared well with the response of CO, reported being adsorbed on the sites with a less ordered structure and edge atoms (semi-crystalline $CuFe_2O_4$) [51]. The signal, above 1900 cm^{-1} (at 200 °C), is also generally ascribed to the formation of carbonyl (CO) on crystalline metal sites [47,48]. The overall shift of CO signals is, in addition to the previously-mentioned coordination strength, partly caused by the temperature-dependent decrease of CO coverage (the weakening of dipole–dipole interactions); nonetheless, it is also, to some extent, a result of the CO desorption from the more labile adsorption sites of the catalysts. DRIFT data indicated that CO, adsorbed on amorphous sites, was less stable and desorbed more easily. At the high temperatures (100–200 °C), the spectra predominantly revealed CO, adsorbed on crystalline domains [49,51].

Raman spectra revealed that neat CNT support possessed a higher crystallinity and graphitization degree, compared to other investigated catalysts (Electronic Supplementary Information, Fig. S3). There were two distinct peaks present, the latter being the D and G band at the wavenumbers of 1340 and 1560 cm^{-1}, respectively [52,53]. In the thermogravimetric analysis (TGA) of the examined catalysts, the weight loss in the temperature range of 200–300 °C could be attributed to the presence of the amorphous carbon on materials' surface, as it is known that such carbonaceous components commence burning in the region of 200–400 °C [52,54]. Conversely, the defect sites in graphite walls and nanotube average diameters influence the oxidative stability of carbon nanotubes (ordered carbon) [55,56]. Furthermore, there was no notable difference in the specific volatilization temperature regions for the CNT-supported metal oxides. After approximately 480 °C, all catalysts exhibited analogous oxidation behaviour with a single-step degradation that indicated the presence of high-purity carbon nanotubes (Electronic Supplementary Information, Fig. S4).

Fig. 4 shows the SEM images of copper based CNT catalysts. It can be observed that they are in the spherical with a diameter of about 1.0–2.0 µm. The images manifest that the copper oxide is in a nano sheet shape and it clearly shows that with the introduction of Co and Fe does not change shape and size of the catalyst. The referential Cu/CNT catalyst without Co and Fe has a similar granular surface as bi-metallic (Fe and Co) supported CNT catalyst. Surface morphology, phase- and

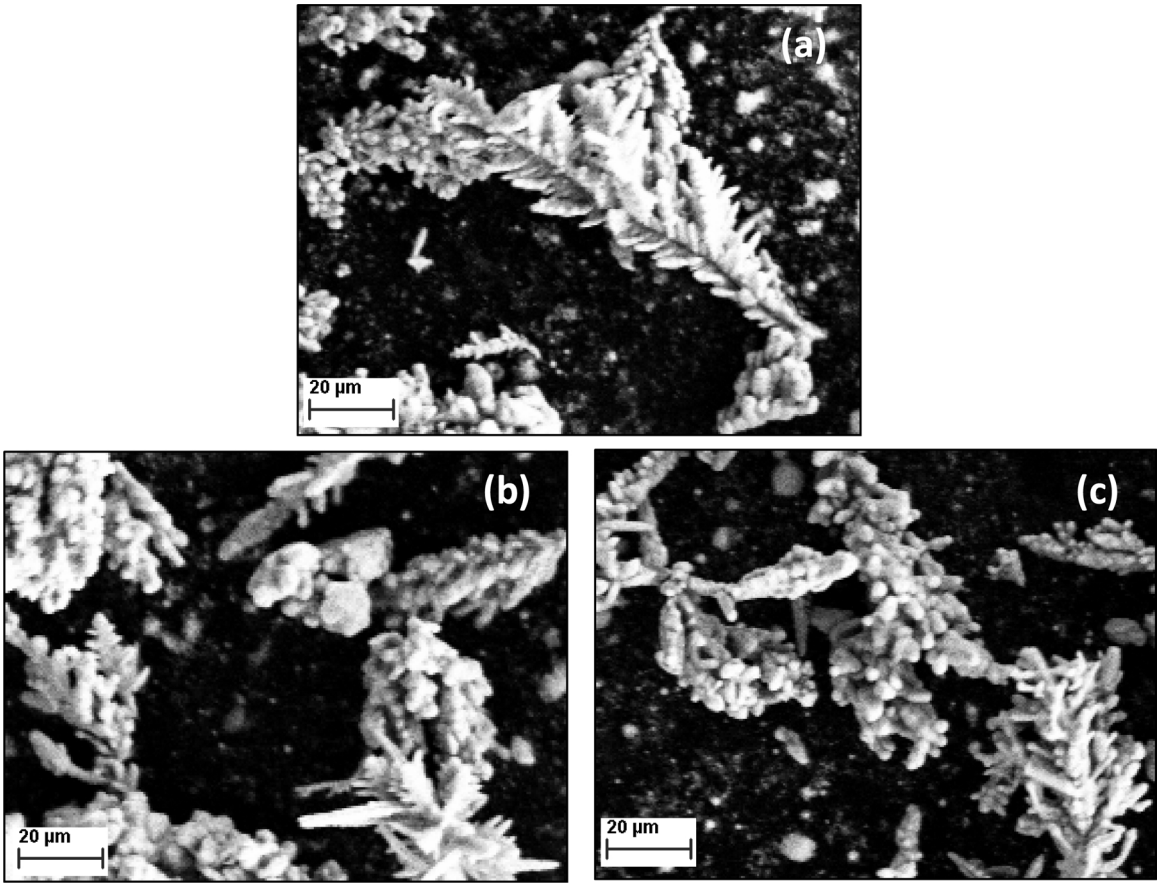

Fig. 4. Scanning Electron Micrographs of Cu/CNT (a), Cu-Fe/CNT (b) and Cu-Co/CNT catalysts.

particle-size distribution was studied by using transmission electron microscopic (TEM) techniques. Fig. 5 presents the microscopic analyses of catalyst samples. As seen in Fig. 5 shows the presence of carbon nanotubes on Cu–Fe/CNT catalyst. Cu–Fe/CNT material showed the round shaped particles of Cu and Fe on the carbon nanotubes, and there was an existence of agglomeration, as well as modular individual particles, which were seen in the obtained structures. All the particles possessed a rough surface morphology (Figs. 4 and 5). The TEM images of Cu–Fe/CNT, conversely, showed that the carbon nanotubes in the range of 10–12 nm width and it is also observed that Cu and Fe were well dispersed on the surface of CNT Energy Dispersive X-ray showed the presence of agglomeration of the copper and iron oxide particles within carbon nanotube support and there were no individual Cu or Fe specks observed. This could be due to occurring of $CuFe_2O_4$ phase, as evidenced by XRD. The EDXS pattern revealed a homogenous distribution of Cu and Fe with particle sizes, ranging from 10 to 18 nm.

The chemical state and relative concentration of the components at the Cu–Fe/CNT catalyst surface was obtained from X-ray photoelectron spectra. Binding energies (BE) were in agreement with the values, reported elsewhere [57]. In XPS spectra (Fig. 6a), two copper species signals were observed; one at 934 eV, corresponding to Cu^{2+} ions in CuO, and another at 943 eV), assigned to the Cu^{2+} ions, dispersed in oxide matrix, specifically, in the spinel environment of $CuFe_2O_4$ [58]. The ratio of the intensity of the shake-up satellite ($I_{sat.}$) to the one of the main Cu $2p_{3/2}$ peak (I_{main}) can be considered as an indicator of the percentage of Cu^{2+}, present in samples. The composition of Cu^{2+} and Cu^{+} varied over a broad range, Cu^{2+} ranging from 0.5 to 0.6 with the remainder of the copper surface being Cu^{+}. XPS spectra of Fe_{2p} (Fig. 6b) showed an intense peak at a high binding energy (BE) of 710.9 eV due to $2p_{3/2}$ accompanied by a satellite line visible at BE of 724.1 eV (due to $2p_{1/2}$). Such a spectral feature, which is can be interpreted as being due to Fe^{3+} in the spinel matrix of $CuFe_2O_4$. The doublet separation was 2.35 eV and the Fe $2p_{3/2}$ and Fe $2p_{1/2}$ peak intensities were in the ratio of 2:1. The intensities of these satellite peaks were 0.35 and 0.40 of the base peak intensity for Fe^{2+} or Fe^{3+}. Of the two peaks Fe $2p_{3/2}$ peak is narrower and stronger than Fe $2p_{1/2}$ and the area of Fe $2p_{3/2}$ peak is greater than that of Fe $2p_{1/2}$ because in spin– orbit (j–j) coupling; Fe $2p_{3/2}$ has degeneracy of four states whilst Fe $2p1_{/2}$ has only two. The peak position of Fe $2p_{3/2}$ has been investigated by many researchers and the values of between 710.6 and 711.2 eV have been reported [57,59].

In the C(1 s) spectral envelopes, there is a presence of five major carbon containing functionalities. The C 1 s envelope is fitted by 5 peaks, C—C, C—O, C═O, O═C—OH, and π-π* shake-up feature. The sp^2 peak of C 1 s envelope is centered at 284.5 eV. The component at 285.2 eV is assigned to C atoms with a single bond to oxygen. The component at 286.3 eV is attributed to carbonyl configuration. The component at 289.1 eV is related to a carboxyl groups. These assignments are in agreement with the literature [60]. Carbon can be bonded to copper or iron titanium through an O (C—O—Cu/Fe) or it can be directly bonded to copper or iron (C—Cu or C—Fe), which, however appears in the range of 280–282 eV [25,60].

The O 1 s curved was mainly composed of metal oxides including Cu—O at 529.9 eV and Cu—O—C at 530.5 eV. The presence of Fe as Fe—O at 529.5 eV. The carbon oxides (C—O) are observed at 532 eV and H—O—H at 533.1 eV. The formation of $CuFe_2O_4$ can be identified by the peak at 280.3 eV in C1 s spectra and 530.5 eV peak in O 1 s along with the peaks at 119.1 eV in the synthesized Cu-Fe/CNT catalysts [61]. The surface ratios of Cu_{2p}/O_{1s} and Fe_{2p}/O_{1s} were in agreement with the nominal ratios of the metal oxides, used for the preparation of catalysts. The surface ratios of Cu/C, Fe/C, and Cu/Fe are in the range of 0.09, 0.04 and 1.8 respectively. This indicates that there is a high amount of

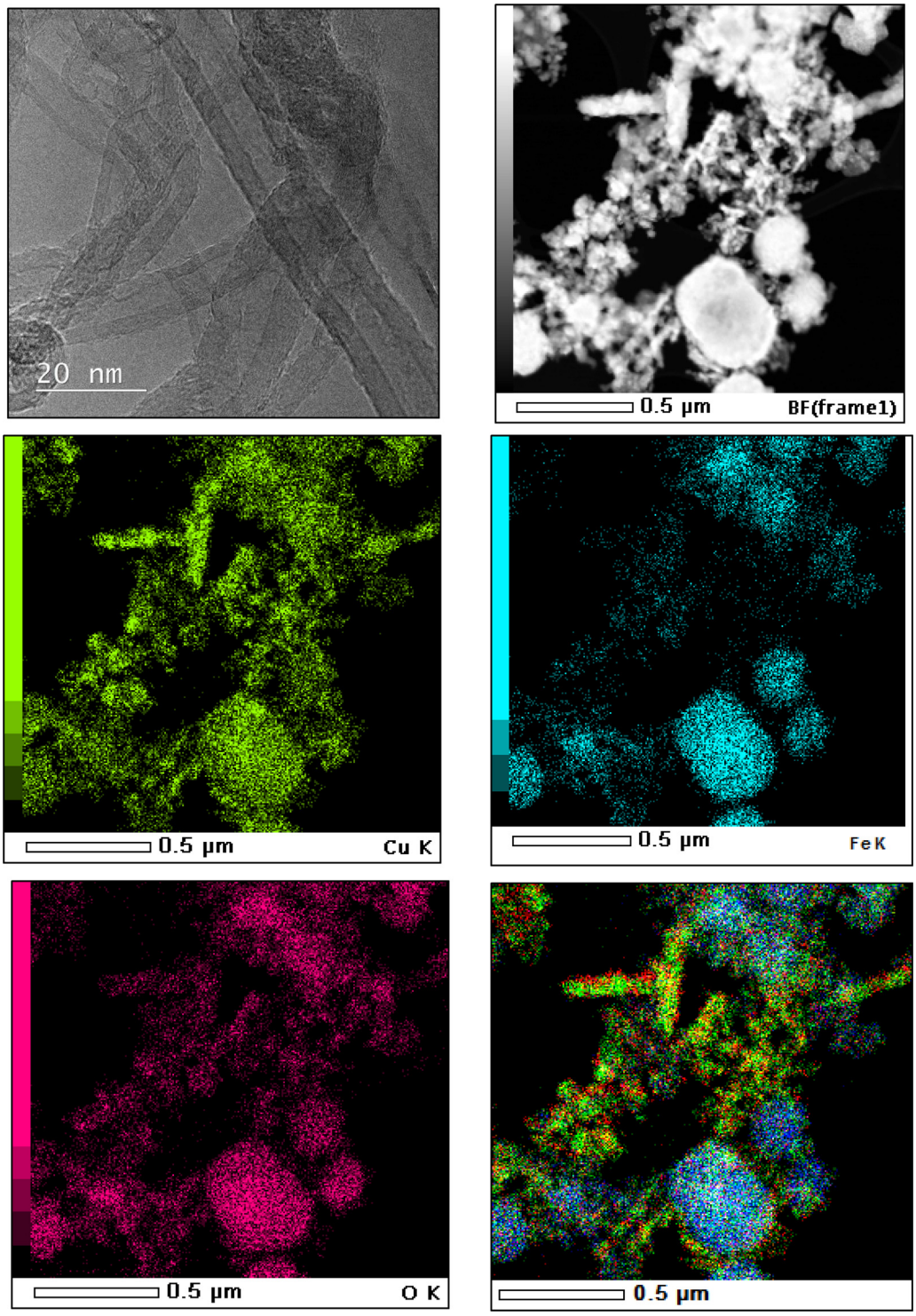

Fig. 5. Transmission Electron Micrograph-Energy dispersive X-ray mapping of Cu, Fe, and overlay of elements over Cu-Fe/CNT catalyst.

Cu on the surface of the catalyst with compared to Fe. The ratio of (Cu + Fe)/CNT is in the range of 0.14 which suggests that there is a high dispersion of Cu-Fe on the surface of CNT [57]. The XPS profile of used Cu-Fe/CNT catalyst (Electronic supplementary information, Fig. S7) also showed the similar profile as fresh catalyst, which is also in agreement with the XRD profile and the stability of the catalyst.

3.2. Catalytic testing

The catalytic activity for the CO oxidation of CNT-supported catalysts was examined at different temperatures up to 220 °C, as shown in Fig. 7. Materials were investigated in the 1 vol. % CO, 1 vol. % O_2 and He (balance) stream at the GHSV of 60,000 h^{-1}. It was observed that Cu–Fe/CNT catalyst performed best. It provided a lower light-off temperature and a 100 mol. % conversion of CO to CO_2 at 180 °C. Cu–Fe/CNT catalyst exhibited a better performance when compared to Cu–Co/CNT and Cu/CNT materials. On the other hand, Co/CNT and Fe/CNT appeared to be less active than all supported copper-containing oxides. This may be due to the strong reduction capacity of Co and Fe with compared to Cu, as marked in TPR profile (Fig. 2). Neat CNT substrate

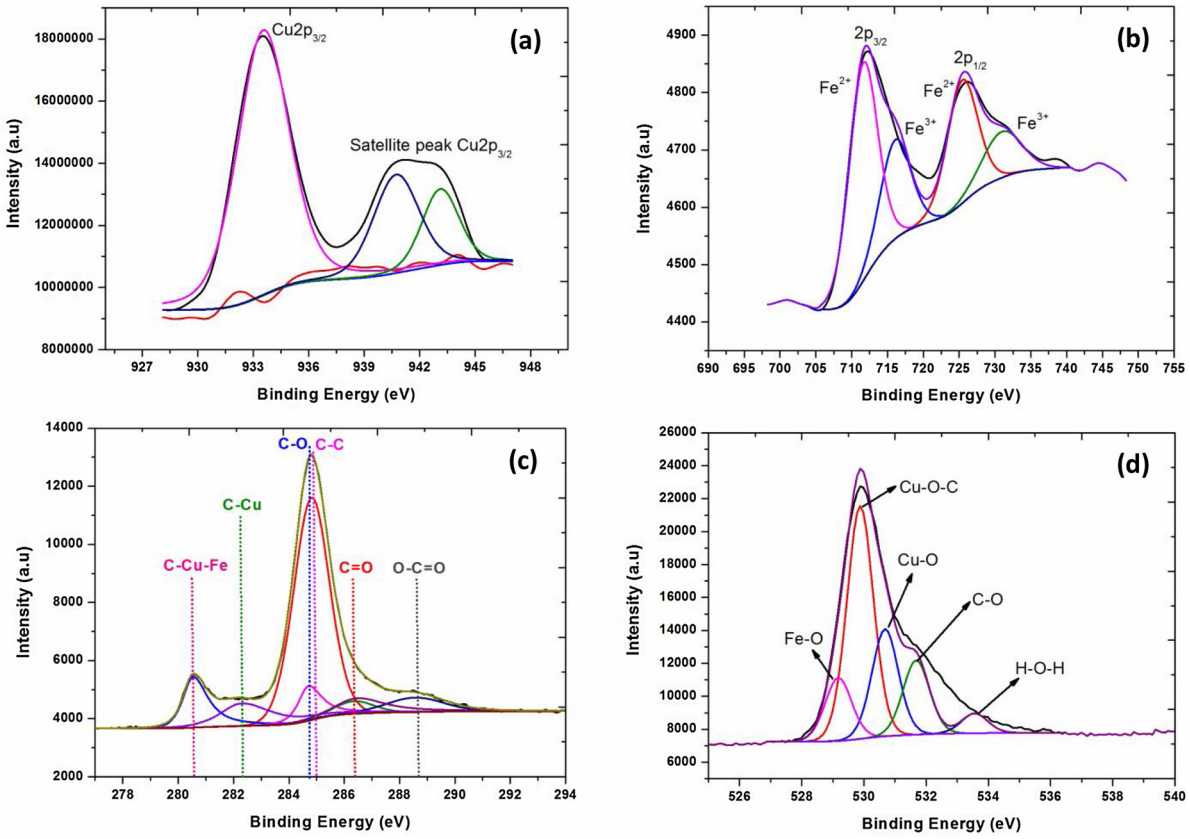

Fig. 6. X-ray photoelectron spectroscopy of Cu-Fe/CNT catalyst in (a) Cu 2p, (b) Fe 2p, (c) C 1 s and (d) O 1 s regions.

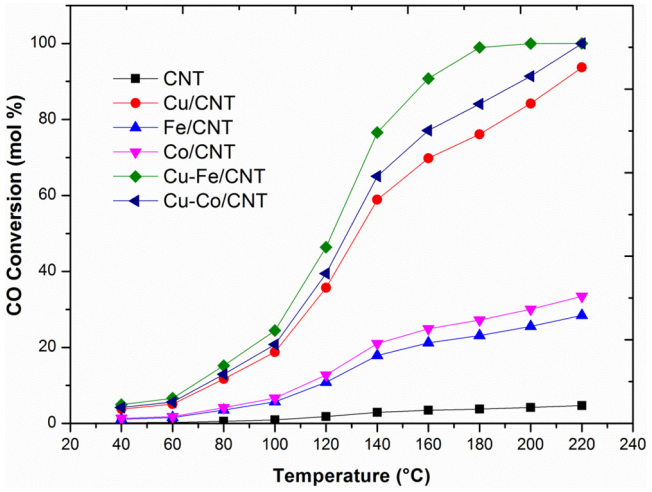

Fig. 7. Variation of CO conversion with reaction temperature over carbon nanotube-supported catalysts (1 vol. % CO, 1 vol. % O_2 and He (balance) mixture at GHSV of 60,000 h^{-1}).

provided a very low CO conversion when compared to CNT-supported materials, and thus, their exerted activity could be mainly attributed to the presence of dispersed active phase(s) on CNT interfaces. The performances with regard to $T_{50\ mol.\ \%}$ (temperature, where 50 mol. % CO conversion is achieved) were sequential as follows: Cu–Fe/CNT (122 °C) < Cu–Co/CNT (127 °C) < Cu/CNT (132 °C) < (Co/CNT, Fe/CNT and CNT (n/a)). As mentioned, this behaviour could be attributed to the reducibility of the employed catalysts, while $T_{50\ mol.\ \%}$ order may be paralleled to TPR profile as well (Fig. 3). These results indicate that the introduction of the Cu species into Co/CNT or Fe/CNT materials can promote the oxidation of CO. Thus, an enhanced catalytic activity could be related to an increased availability of CO-accessible surface sites due to the incorporation of CuO [22,50]. A pure $CuFe_2O_4$ showed a deactivation trend after 2 h of reaction time. In this short period, it showed a high activity (100% CO Conversion). Thus, with the introduction of CNT as a support to Cu-Fe catalysts, the stability and the activity of the catalyst increased.

A typical composition of the effluent gas from a water–gas shift reactor contains approximately 1 mol. % of CO in a large excess of H_2 [23]. Thus, PROX process involves two global competitive reactions, these being the oxidation of carbon monoxide and hydrogen. Since PROX operation unit is positioned between a low-temperature shift reactor (~200 °C) and PEM FC (~80 °C), the catalyst for PROX should for an efficient use of energy work between the two operating temperatures as well. Meanwhile, the start-up at low temperatures (*e.g.* the ambient temperature) is also quite important for the automotive applications of fuel cells [1]. Thus, an efficient PROX catalyst is in overall required to exhibit a good performance over a wide temperature range [24]. Fig. 6 depicts the evolution of CO conversion and the selectivity towards CO_2 for the CNT support and examined catalysts for a realistic feedstock. It can be seen that a neat CNT support did not exhibit any significant activity for the CO oxidation by PROX reaction. This observation is also supported by the literature [22,24], implying that CNT exert very poor in activity, even as high as 300 °C. Monometallic Co and Fe, supported on CNT, exhibited a lower conversion in CO oxidation than Cu/CNT catalyst, which occurred due to the easily-reducible nature of the copper species on the surface of CNT. The CO consumption for all samples was considerably decreased by the introduction of H_2, while it presented a similar trend as in pure CO oxidation. CO_2 formation declined gradually from over 90 mol. % to under 10 mol. % with an increase in temperature. As compared to CO conversion, CO_2 selectivity also showed an analogous trend.

CNT-supported monometallic Co or Fe catalysts, when compared to Cu-containing materials, exhibited a poorer CO PROX performance

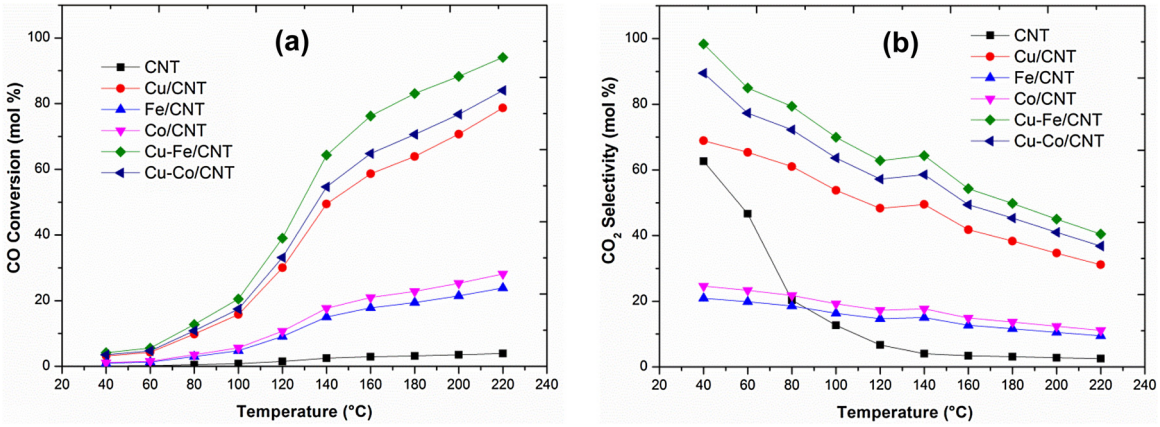

Fig. 8. Variation of CO conversion (a) and CO_2 selectivity (b) with reaction temperature over carbon nanotube-supported catalysts (1 vol. % CO, 1 vol. % O_2, 60 vol. % H_2 and He (balance) mixture at GHSV of 60,000 h^{-1}).

under identical conditions (Fig. 8). Furthermore, at relatively high temperatures (180–220 °C), copper-based composites demonstrated the maximal CO_2 selectivity in the range of 30–50 mol. %, which was higher than that of monometallic Co or Fe. CO conversion over Cu-containing catalysts thus monotonically increased with temperature, indicating that Cu species tended to be active with CO, in this case exhibiting a high rate as well. The reverse WGS reactions were not observed over the CNT-supported materials, which could be due to the high adsorption energy of CO_2, as also substantiated by the literature [22,24,62]. Therefore, the promotional effect of Cu for CO PROX may have been attributed to the formation of minor CO-containing oxidizing species, such as carboxyl groups, which could selectively oxidise a CO molecule in H_2-rich stream [15,23,63]. At relatively high temperatures, the generation of excess oxidising −OH moieties brings about a drop in CO_2 selectivity, leading to a poorer CO PROX performance. A high conversion towards CO_2 can be attributed to the presence of $CuFe_2O_4$ on Cu–Fe/CNT, and the synergistic effect between Cu and Co in Cu–Co/CNT catalysts (Figs. 1 and 2).

Contact time has been reported to have an important role in CO PROX reactions due to the parallel oxidation of hydrogen. In this work, the influence of feedstock residence was investigated by varying the volumetric feed flow rate in terms of GHSV. The effect of space velocity was investigated in the range of 30000–90000 h^{-1}. It could be noticed that with an increase in GHSV, the conversion of CO decreased, as well as the selectivity towards CO_2 (Fig. 9) (Electronic Supplementary Information, Fig. S5). Prolonged contact time also pronounced the undesired parallel oxidation of hydrogen to water, and thus, hydrogen conversion exhibited an inverse trend to CO oxidation. A noticeable feature of the reactions of hydrogen was that neat CNT themselves granted a high H_2 turnover when compared to CNT-supported metal oxide catalysts. The latter could be due to the formation of minor hydrogen-containing oxidising species, such as hydroxyl group, which could further produce water. These results indicate that the influence of the space velocity on CO PROX was significant; however, an almost complete removal of CO was obtainable at moderate space velocities (*e.g.* Figs. 6 and 7). Lastly, there was no major effect of the GHSV on oxygen conversion.

The existing literature on the preferential CO oxidation reactions in the presence of H_2 reports using gas mixtures, comprising of CO, O_2 and H_2 [64]. Conversely, such a feed does not absolutely simulate the realistic conditions of an arbitrary reforming system, as beside the stated gases, there is also a certain quantity of H_2O and CO_2, existent in the initial mixture [24]. Thus, the effect of the H_2O and CO_2 addition into a feedstock was studied over the carbon nanotube-based catalysts. The results obtained, in terms of CO conversion as a function of reaction temperature, are presented in Fig. 10. The presence of CO_2 in feed gas yielded a minor decrease of the catalytic activity over operating temperatures; still, an increase in the CO reactions extent over temperature was observed. However, it has also been reported that the occurrence of CO_2 in a feedstock stream inhibited CO oxidation due to the formation of the carbonates on a metal oxide surface, owing to the adsorption of CO_2, which led to the deactivation of catalysts' redox properties [54]. At high temperatures, the CO_2 binding effect is additionally clearly reduced, which may explain an increase in the catalytic activity over temperature (analogous to the one without CO_2). Furthermore, a decrease in the formation of CO_2 from CO was observed at relatively high temperatures (not shown), which has been noted in various studies [54,27,16,17]. As reported in the literature, the presence of CO_2 acts through disrupting prevalent reaction mechanisms due to the alteration of the distribution of products, adsorbed on metal oxide catalysts [14,15,65]. The present results also indicated that CO_2 exhibited a promoting effect on H_2 oxidation, decreasing CO conversion (Fig. 10).

Moreover, regarding the effect of CO_2 addition, CO conversion below the temperature of 100 °C did not vary notably whether CO_2 was added or not; nonetheless, as the temperature rose above 120 °C, CO turnover clearly decreased (Fig. 10). O_2 consumption exhibited behaviour, similar to that of CO, while above 120 °C, O_2 reactions' extent reached 100 mol. %. However, CO_2 selectivity decreased by increasing reaction temperature. A probable reason for the lowering CO oxidative activity and selective CO_2 production with elevated temperature could have been sought in more pronounced reverse water–gas shift reactions.

The reformed gas, supplied for the PROX reactions after the WGS in realistic processes, also contains H_2O, which alters catalyst activity [14,24,62]. The water addition to gaseous stream thus affected the catalytic performance of carbon nanotube-supported materials. The results indicated that the existence of the −OH groups on the substrate surface may have promoted conversion activity. Therefore, when H_2O was added, CO consumption increased, more notably after 100 °C, and exhibited a 100 mol. % reactions' extent in the range of 200–220 °C for Cu–Fe/CNT (Fig. 8). Compared to the results in the absence of any H_2O or CO_2 addition, catalyst activity improved with an increase in temperature when adding H_2O. The latter was in agreement with the literature [20,24]; specifically, indicating that the presence of H_2O decreases the apparent activation energy of CO and H_2 oxidation so that CO conversion increases significantly without any drastic change in CO_2 selectivity. As mentioned, the latter could be due to hydroxyl groups, forming on the catalyst surface by the dissociative adsorption of H_2O, which in turn acted as a better oxidant than O_2, thereby elevating CO and H_2 consumption rates, and thus, the CO depletion over process temperature as well (Fig. 10).

In the case of a combined presence of H_2O and CO_2 in the feed stream, an adverse effect on catalytic activity was observed (Fig. 8)

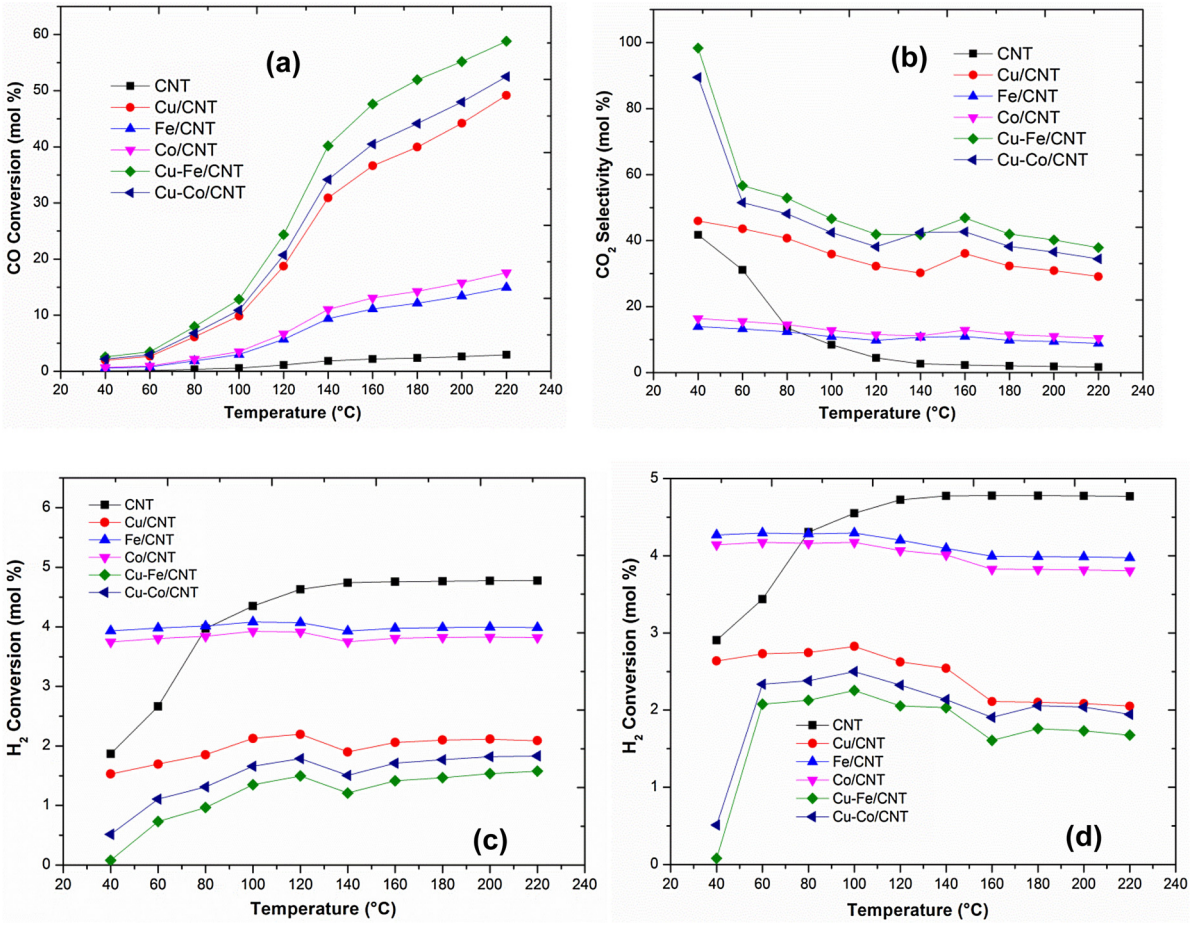

Fig. 9. Variation of CO conversion (a) and CO_2 selectivity (b) with reaction temperature over carbon nanotube-supported catalysts (1 vol. % CO, 1 vol. % O_2, 60 vol. % H_2 and He (balance) mixture at GHSV of 90,000 h^{-1}). Variation of H_2 conversion with reaction temperature over carbon nanotube supported-catalysts at GHSV of 60,000 h^{-1} (c) and 90,000 h^{-1} (d) (1 vol. % CO, 1 vol. % O_2, 60 vol. % H_2 and He (balance) mixture).

which may have been ascribed to the competitive adsorption on metal oxide active sites. Analogous results have been found for other systems, which has been previously reported in the literature [66]; specifically, the performance of Pt/CeO_2 catalysts was greatly affected by introducing both H_2O and CO_2 and this influence exhibited a dependency on the reaction temperature. At relatively low temperatures, catalytic activity decreased over platinum materials; nevertheless, this effect was negligible at higher temperatures. The effective negative influence of H_2O and CO_2 in feed was surmised to have occurred due to the formation of the specific carbonate species at interfacial sites and the blockage of the active centres by adsorbed water molecules (surpassing promoting hydroxyl production), whereas this was reported to occur extensively at low temperatures [20,24].

One of the most important requirements for PROX catalysts is that they have to operate in a relatively wide temperature range and exhibit a good resistance to deactivation, caused by H_2O and CO_2 in a feed [24,50,63]. The presence of CO_2 in a feedstock will, as mentioned, result in the formation of carbonates and carbonyls during surface reactions, which further decrease the activity for CO oxidation. Thus, a proper catalyst has to be also examined with regard to longer-term stability. Fig. 8 shows the activity of the materials under H_2O, CO_2, and a combined H_2O and CO_2 feed. The fabricated carbon nanotube-supported catalysts exhibited a stable CO conversion for more than 260 min. The same stability was also observed in terms of CO_2 selectivity. The activity conservation of the catalysts in the presence of 10 vol. % H_2O did not differ from that, monitored in the absence of H_2O under the same conditions, as CO conversion and CO_2 production remained constant for more than 260 min.

H_2O and CO_2, present in the feed stream of an actual PROX reactor were found to affect the performance of PROX catalysts, as mentioned above, whereas, for the supported platinum materials, the apparent activation energy of CO oxidation was reduced from 74 kJ mol^{-1}, obtained in the absence of H_2O, to 37 kJ mol^{-1} [67]. The same trend was observed over the carbon nanotube-based composites. The apparent activation energies of the CO oxidation under different feed conditions were calculated using the Arrhenius equation (Electronic Supplementary Information, Fig. S6). The activation energy of the CO conversion over Cu–Fe/CNT in the absence of H_2O and CO_2 was found to be 58 kJ mol^{-1}, which decreased to 36 kJ mol^{-1} upon the presence of H_2O in the feed. The latter could be due to H_2O blocking H_2 adsorption and allowing for the preferential CO oxidation at higher temperatures to proceed at high rates. The activation energy of CO conversion increased to 81 kJ mol^{-1} and 63 kJ mol^{-1} for CO_2-, or a combined H_2O- and CO_2-containing feed.

Cu-based oxide catalysts, that are considered a highly desirable material for CO PROX due to their good catalytic performances and low production costs, could become an alternative to their precious metal analogs of the past decade [15]. Cu–Ce, in which the interface between CuO and CeO_2 support plays an important role in CO oxidation activity was extensively studied in CO PROX reactions [49,50]. However, this Cu–Ce catalysts exhibit a rather low efficiency when compared to Cu/CNT materials (Figs. 6 and 7), applied for CO PROX in the operating temperature range of 100–200 °C. Cu/CNT composite demonstrated a high metal dispersion and CO amount, chemisorbed on its surface (Table 2), which led to an elevated rate of CO conversion. Cu/CNT catalyst also exhibited a very stable activity over longer times, with and

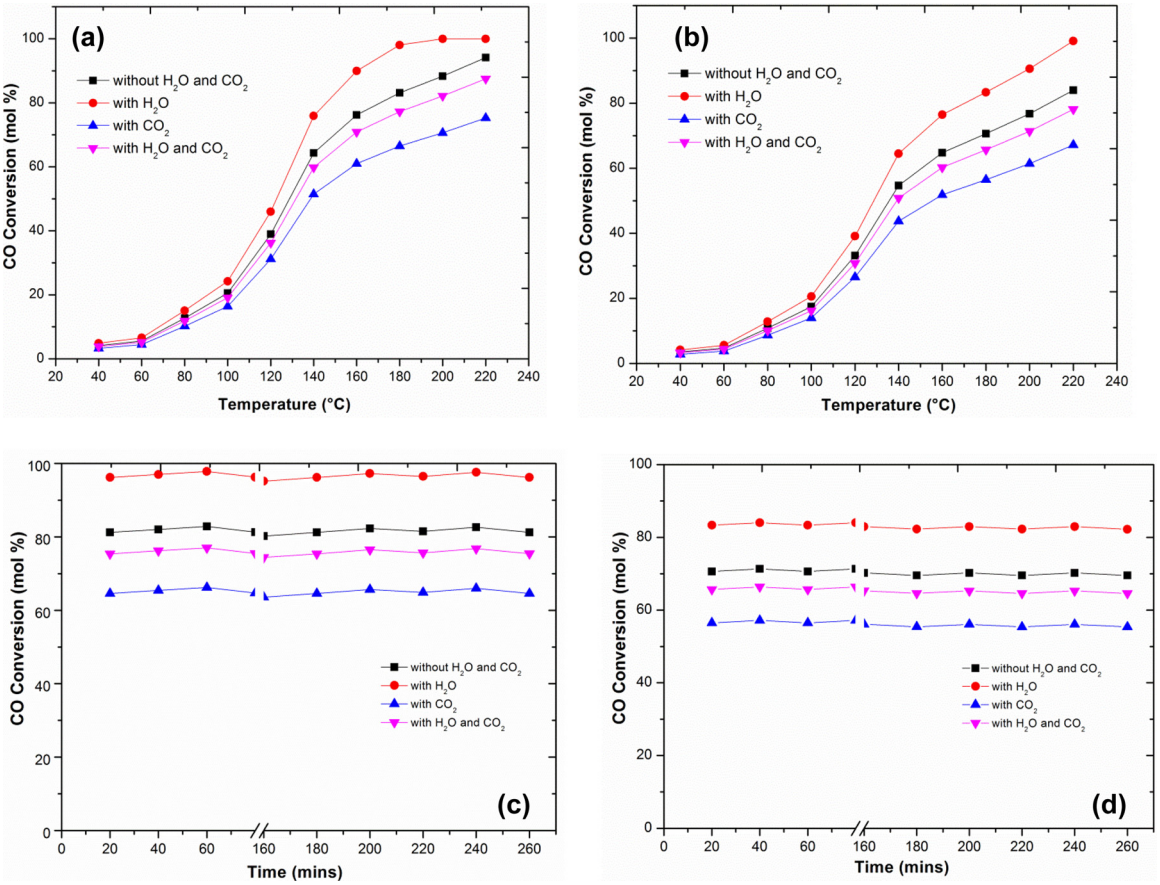

Fig. 10. Variation of CO conversion with reaction temperature over Cu–Fe/CNT (a) and Cu–Co/CNT (b) catalysts (1 vol. % CO, 1 vol. % O_2, 0–10 vol. % H_2O, 0–10 vol. % CO_2, 40–60 vol. % H_2 ($H_2O/CO_2/H_2$ tot. 60 vol. %) and He (balance) mixture at GHSV of 60,000 h^{-1}). Variation of CO conversion with time over Cu–Fe/CNT (c) and Cu–Co/CNT (d) catalysts at reaction temperature of 180 °C (1 vol. % CO, 1 vol. % O_2, 10 vol. % H_2O, 20 vol. % CO_2, 60 vol. % H_2 and He (balance) mixture at GHSV of 60,000 h^{-1}).

Table 3
Rate of CO conversion ($mmol_{CO}$ s^{-1} $kg_{cat.}^{-1}$) over carbon nanotubes (1 vol. % CO, 1 vol. % O_2, 10 vol. % H_2O, 20 vol. % CO_2, 60 vol. % H_2 and He (balance) mixture at GHSV of 60,000 h^{-1} and temperature of 200 °C).

Catalyst	Without H_2O/CO_2	With H_2O	With CO_2	With H_2O/CO_2
CNT	0.13	0.15	0.10	0.12
Cu/CNT	2.56	3.02	2.05	2.38
Co/CNT	0.91	1.08	0.73	0.85
			732.66	
Fe/CNT	0.78	0.92	0.62	0.72
Cu–Co/CNT	2.83	3.33	2.26	2.63
Cu–Fe/CNT	3.32	3.92	2.66	3.09

without input H_2O and CO_2. On the other hand, Co/CNT and Fe/CNT materials demonstrated a very low rate of CO conversion; nonetheless, they also displayed a long-term stability (Fig. 8). Moreover, the rates of CO consumption corresponded to catalysts' metal dispersion and desorption profiles (Table 3).

In the literature [19,20], it has been reported that iron(III) oxide catalysts exhibit analogous characteristics as CeO_2 [65,68], and it was found that Fe^{3+} had a promotional effect due to the electron changes between Cu^{2+}/Fe^{3+} and Ce^{4+}/Ce^{3+}. The high activity of these catalysts is attributed to synergistic interaction of Cu and Ce along with Cu and Fe interfacial sites, which is similar to the effect on the activity of CuO-based materials similar to Ce^{3+}, applied to CO oxidation [20,64]. The investigation of the CO consumption over iron oxides, which were calcined at different temperatures [12,69], indicated that a highly-active CO conversion catalyst was formed after the calcination at 400 °C. The realization of a synergistic effect occurred due to the interaction between copper and iron species and the formation of $CuFe_2O_4$ [19,20,70]. The Cu-Fe interaction helps stabilize and greatly improve the dispersion of Cu° and thus enhances the CO conversion [41]. Cu–Fe mixed oxide catalysts, that exhibited a higher CO oxidation activity and selectivity towards CO_2 in comparison to individual CuO and Fe_2O_3 materials, have been suggested as an alternative to their precious metal analogs [49,50] due to their low production costs and a ready availability of the starting materials. They are thus in a better competitive position than the precious metal- and Cu–Ce-based alternatives [20,28,48,63], especially when targeting mass market application.

CNT play an improving role considering catalytic performance and resistance against CO_2 and H_2O *via* increasing the number of active sites and the concentration of the oxygen vacancies in the case of CeO_2/CNTs–CuO catalysts. In addition to the effect of support, the synergistic interaction between Pt metal surface and CoO are largely responsible for an enhanced CO PROX performance of Pt-Co/CNT. Moreover, CeO_2 addition to Pt/CNT catalyst further improves catalytic activity and selectivity (the CO conversion rate of 3.95 $mmol_{CO}$ s^{-1} $kg_{cat.}^{-1}$) [68], the material's influence being superior to that exhibited by traditional PROX analogs, such as Pt/CeO_2 (the rate of 2.81) [66], which contain many critical resources, such as platinum or Ce.

In the present study, Cu–Fe/CNT catalyst exhibited a high rate of CO conversion (with and without H_2O and CO_2) when compared to Cu/CNT and Fe/CNT materials (Table 3). As noted, a high activity and selectivity were caused by the effect of the interactions between the main phases of delafossite, $CuFe_2O_4$ and Fe_2O_3 [20,27,51,66]. Cu–Co/CNT bimetallic catalysts also exhibited a substantial rate of CO

Table 4
Rate of CO conversion ($mmol_{CO}\ s^{-1}\ kg_{cat.}^{-1}$) over various metals supported on carbon nanotubes at 200 °C.

Catalyst	Rate of CO conversion ($mmol_{CO}\ s^{-1}\ kg_{cat.}^{-1}$)	Reference
2% Pt/CNT	2.22	[71]
2% Pt/Ce/CNT	2.85	[72]
4% Pt/Ni/CNT	2.93	[71]
2% Co–4% Pt/CNT	2.98	[24]
9% Cu–1% Ce/CNT	2.51	[20,68]
5 % Ru/CNT	2.62	[73]
8% Cu–1%Co/CNT	1.52[a]	[39]
10% Cu–5 %Co/CNT	2.83	This work
10 %Cu– 5 % Fe/CNT	3.32	This work

[a] with out H_2O and CO_2 in feed.

conversion when compared to Cu/CNT and Co/CNT materials. The promotional effect of Cu was evidenced by an increase in the adsorption capacity of the composite (Table 2) and a decrease in peak reduction temperature.

In comparison to the other CNT-based catalysts for PROX reaction, reported in the literature [20,28,65], Cu–Fe/CNT material exhibited a high activity. These catalysts showed an enhanced performance when compared to the analogs, consisting of Ce and Pt (Table 4). There are two kinds of metal species, one interacting with ceria or platinum, and likely to form the Ce–M or Pt–M alloy in reduction process, and the other being much more dispersed on carbon nanotubes and strongly interacting with the supports [68,71,72]. Considering these studies, it was also found that the strong interaction between active copper species (predominantly Cu^+) and reducible support (such as Fe_2O_3 and CeO_2) is a prerequisite for a good performance in CO oxidation. A high activity might have therefore arisen on account of small Cu^+ clusters, which were formed *in situ* under hydrothermal conditions due to the chemical reactions with CNT substrate [14,15,22,50]. Moreover, under CO PROX process conditions, Cu was found to exist mainly as Cu^+. Wu and co-workers [74] showed that an iron promoter effectively improves the reaction conversion and stability of the Cu/SiO_2 catalyst. Rather than the oxidation of copper, the Fe species in the $Cu–Fe/SiO_2$ catalyst is oxidised by the reaction feed, while the oxidation of metallic Cu° can be inhibited. Analogously to CuO systems, reported in the literature [12,49,65,75], Cu composite catalysts, presented in this work, have shown a high relative activity for CO oxidation and a strong interaction between the two metal components, believed to be responsible for the said good performance, stability-wise as well.

4. Conclusions

1 A high selectivity and conversion in the preferential oxidation of CO in the presence of a large quantity of CO_2, H_2 and H_2O have demonstrated on the carbon nanotube-supported catalysts for the temperatures between 120 and 200 °C. With simulated water–gas shift reaction product stream containing 1 vol. % CO and a varying amount of CO_2, H_2 and H_2O, Cu–Fe/CNT catalysts were able to achieve 100% CO conversions at the temperature of 220 °C, using an excess amount of O_2 (1 vol. %). The high selectivity towards CO_2 can be attributed to the presence of $CuFe_2O_4$ on CNT and the synergistic effect of Co and Cu in Cu–Co/CNT catalysts.
2 The apparent activation energy for the CO oxidation over Cu–Fe/CNT was 58 kJ mol^{-1}, which decreased to 36 kJ mol^{-1} in the presence of H_2O in the feedstock applied. The latter could be due to H_2O interacting with the surface and CO during CO chemisorption and increasing the preferential CO oxidation at higher temperatures as well, where PROX rates were respectively higher. The apparent activation energy of CO oxidation increased to 81 kJ mol^{-1} with CO_2 in the feedstock applied and dropped to 63 kJ mol^{-1} upon a combined CO_2 and H_2O presence. The outlet concentration of CO at the maximum conversion level is in the range of 2–6 ppm.
3 The other bimetallic catalysts, presented in this study, *i.e.* Co–Cu/CNT, also showed a high rate of CO conversion when compared to Co/CNT and Cu/CNT material. The promotional effect of Cu was evidenced by an increase in the desorption capacity of these catalysts and a decrease in its mean reduction temperature.
4 Cu/CNT catalyst also showed a very stable activity over longer time both with CO_2 and H_2O present. On the other hand, Co/CNT and Fe/CNT materials exhibited a very low rate of CO conversion; nonetheless, these catalysts also showed an adequate long-term stability. The mentioned rates were in agreement with the metal dispersion and desorption profile of the materials examined.
5 In comparison to the catalyst systems (except Ce and Pt), reported insofar, the Cu composite material, presented in this work, has shown a high activity for CO oxidation, while the strong interaction between the two metal components employed is believed to be responsible for this behaviour.

Acknowledgements

The authors acknowledge the financial support from the Slovenian Research Agency (research core funding No. P2–0152), and the project “Direct Conversion of Methane to Higher Hydrocarbons Using Superacid Catalysts” (J2-7319) which was financially supported by the Slovenian Research Agency. The authors would also like to thank Dr. Janez Kovač for XPS measurements and discussions. The authors also acknowledge Assist. Prof. Dr. Ivan Jerman for the assistance in Raman spectroscopy studies.

Appendix A. Supplementary data

Supplementary material related to this article can be found, in the online version, at doi:https://doi.org/10.1016/j.apcatb.2018.06.069.

References

[1] İ. Dinçer, C. Zamfirescu, Hydrogen and Fuel Cell Systems, Sustainable Energy Systems and Applications, Springer, US, 2012, pp. 519–632.
[2] B. Sørensen, Hydrogen and Fuel Cells: Emerging Technologies and Applications, Academic Press, 2012.
[3] T.R. Ralph, M.P. Hogarth, Catalysis low temperature fuel cells, Platinum Met. Rev. 46 (2002) 117–135.
[4] F.J. Barclay, Fuel Cells, Engines and Hydrogen: An Exergy Approach, Wiley, 2006.
[5] D. Bessarabov, H. Wang, H. Li, N. Zhao, PEM Electrolysis for Hydrogen Production: Principles and Applications, CRC Press, 2016.
[6] H. Wang, X.Z. Yuan, H. Li, PEM Fuel Cell Diagnostic Tools, Taylor & Francis, 2011.
[7] X.Y. Liu, A. Wang, T. Zhang, C.-Y. Mou, Catalysis by gold: new insights into the support effect, Nano Today 8 (2013) 403–416.
[8] M.M. Schubert, S. Hackenberg, A.C. van Veen, M. Muhler, V. Plzak, R.J. Behm, CO oxidation over supported Gold catalysts—“inert” and “active” support materials and their role for the oxygen supply during reaction, J. Catal. 197 (2001) 113–122.
[9] D. Takagi, Y. Kobayashi, H. Hibino, S. Suzuki, Y. Homma, Mechanism of Gold-catalyzed carbon material growth, Nano Lett. 8 (2008) 832.
[10] T. Chetty, H.B. Friedrich, V.D.B.C. Dasireddy, A. Govender, P.J. Mohlala, W. Barnard, Effect of various Au/Al2O3 preparations on catalytic behaviour during the continuous flow hydrogenation of an octanal/octene mixture, ChemCatChem 6 (2014) 2384–2393.
[11] A. Villa, S. Campisi, K.M.H. Mohammed, N. Dimitratos, F. Vindigni, M. Manzoli, W. Jones, M. Bowker, G.J. Hutchings, L. Prati, Tailoring the selectivity of glycerol oxidation by tuning the acid-base properties of Au catalysts, Catal. Sci. Technol. 5 (2015) 1126–1132.
[12] P.-P. Du, W.-W. Wang, C.-J. Jia, Q.-S. Song, Y.-Y. Huang, R. Si, Effect of strongly bound copper species in copper–ceria catalyst for preferential oxidation of carbon monoxide, Appl. Catal., A 518 (2016) 87–101.
[13] F. Mariño, C. Descorme, D. Duprez, Noble metal catalysts for the preferential oxidation of carbon monoxide in the presence of hydrogen (PROX), Appl. Catal., B 54 (2004) 59–66.
[14] C.A. Chagas, E.F. de Souza, R.L. Manfro, S.M. Landi, M.M.V.M. Souza, M. Schmal, Copper as promoter of the NiO–CeO2 catalyst in the preferential CO oxidation, Appl. Catal., B 182 (2016) 257–265.
[15] A. Arango-Díaz, J.A. Cecilia, E. Moretti, A. Talon, P. Núñez, J. Marrero-Jerez, J. Jiménez-Jiménez, A. Jiménez-López, E. Rodríguez-Castellón, Comparative study of CuO supported on CeO2, Ce0.8Zr0.2O2 and Ce0.8Al0.2O2 based catalysts in the CO-PROX reaction, Int. J. Hydrogen Energy 39 (2014) 4102–4108.
[16] F. Studt, M. Behrens, F. Abild-Pedersen, Energetics of the water–gas-shift reaction

on the active sites of the industrially used Cu/ZnO/Al2O3 catalyst, Catal. Lett. 144 (2014) 1973–1977.
[17] T.L. LeValley, A.R. Richard, M. Fan, The progress in water gas shift and steam reforming hydrogen production technologies – a review, Int. J. Hydrogen Energy 39 (2014) 16983–17000.
[18] A.A. Gokhale, J.A. Dumesic, M. Mavrikakis, On the mechanism of low-temperature water gas shift reaction on copper, J. Am. Chem. Soc. 130 (2008) 1402–1414.
[19] T. Tabakova, G. Avgouropoulos, J. Papavasiliou, M. Manzoli, F. Boccuzzi, K. Tenchev, F. Vindigni, T. Ioannides, CO-free hydrogen production over Au/CeO2–Fe2O3 catalysts: part 1. Impact of the support composition on the performance for the preferential CO oxidation reaction, Appl. Catal., B 101 (2011) 256–265.
[20] G. Avgouropoulos, T. Ioannides, C. Papadopoulou, J. Batista, S. Hocevar, H.K. Matralis, A comparative study of Pt/γ-Al2O3, Au/α-Fe2O3 and CuO–CeO2 catalysts for the selective oxidation of carbon monoxide in excess hydrogen, Catal. Today 75 (2002) 157–167.
[21] S.F. Yin, B.Q. Xu, W.X. Zhu, C.F. Ng, X.P. Zhou, C.T. Au, Carbon nanotubes-supported Ru catalyst for the generation of COx-free hydrogen from ammonia, Catal. Today 93–95 (2004) 27–38.
[22] S. Zeng, L. Zhang, N. Jiang, M. Gao, X. Zhao, Y. Yin, H. Su, Multi-wall carbon nanotubes as support of copper–cerium composite for preferential oxidation of carbon monoxide, J. Power Sources 293 (2015) 1016–1023.
[23] Y. Gao, K. Xie, S. Mi, N. Liu, W. Wang, W. Huang, Preferential oxidation of CO in a H2-rich stream over multi-walled carbon nanotubes confined Ru catalysts, Int. J. Hydrogen Energy 38 (2013) 16665–16676.
[24] C. Wang, B. Li, H. Lin, Y. Yuan, Carbon nanotube-supported Pt-Co bimetallic catalysts for preferential oxidation of CO in a H2-rich stream with CO2 and H2O vapor, J. Power Sources 202 (2012) 200–208.
[25] B. Gao, G.Z. Chen, G. Li Puma, Carbon nanotubes/titanium dioxide (CNTs/TiO2) nanocomposites prepared by conventional and novel surfactant wrapping sol–gel methods exhibiting enhanced photocatalytic activity, Appl. Catal., B 89 (2009) 503–509.
[26] S. Lambert, C. Cellier, P. Grange, J.-P. Pirard, Bt. Heinrichs, Synthesis of Pd/SiO2, Ag/SiO2, and Cu/SiO2 cogelled xerogel catalysts: study of metal dispersion and catalytic activity, J. Catal. 221 (2004) 335–346.
[27] V. Perrichon, L. Retailleau, P. Bazin, M. Daturi, J.C. Lavalley, Metal dispersion of CeO2–ZrO2 supported platinum catalysts measured by H2 or CO chemisorption, Appl. Catal., A 260 (2004) 1–8.
[28] W.-W. Wang, P.-P. Du, S.-H. Zou, H.-Y. He, R.-X. Wang, Z. Jin, S. Shi, Y.-Y. Huang, R. Si, Q.-S. Song, C.-J. Jia, C.-H. Yan, Highly dispersed copper oxide clusters as active species in copper-ceria catalyst for preferential oxidation of carbon monoxide, ACS Catal. 5 (2015) 2088–2099.
[29] K. Dai, X. Zhang, K. Fan, P. Zeng, T. Peng, Multiwalled carbon nanotube-TiO2 nanocomposite for visible-light-induced photocatalytic hydrogen evolution, J. Nanomater. 2014 (2014) 8.
[30] J. Lin, C. Chen, M. Rummeli, A. Bachmatiuk, Z. Zeng, H. Ma, B. Buchner, H. Chen, Growth of carbon nanotubes catalyzed by defect-rich graphite surfaces, Chem. Mater. 23 (2011) 1637–1639.
[31] F. Li, Y. Wang, D. Wang, F. Wei, Characterization of single-wall carbon nanotubes by N2 adsorption, Carbon 42 (2004) 2375–2383.
[32] K.S.W. Sing, D.H. Everett, R.A.W. Haul, L. Moscou, R.A. Pierotti, J. Rouquerol, T. Siemieniewska, Pure Appl. Chem. 57 (1985) 603–619.
[33] G.V. Sagar, P.V.R. Rao, C.S. Srikanth, K.V.R. Chary, Dispersion and reactivity of copper catalysts supported on Al2O3 − ZrO2, J. Phys. Chem. B 110 (2006) 13881–13888.
[34] Š. Hajduk, V.D.B.C. Dasireddy, B. Likozar, G. Dražić, Z.C. Orel, COx-free hydrogen production via decomposition of ammonia over Cu–Zn-based heterogeneous catalysts and their activity/stability, Appl. Catal., B 211 (2017) 57–67.
[35] V.D.B.C. Dasireddy, B. Likozar, Selective catalytic reduction of NOx by CO over bimetallic transition metals supported by multi-walled carbon nanotubes (MWCNT), Chem. Eng. J. 326 (2017) 886–900.
[36] H. Guo, H. Zhang, F. Peng, H. Yang, L. Xiong, C. Wang, C. Huang, X. Chen, L. Ma, Effects of Cu/Fe ratio on structure and performance of attapulgite supported CuFeCo-based catalyst for mixed alcohols synthesis from syngas, Appl. Catal., A 503 (2015) 51–61.
[37] R. Lu, D. Mao, J. Yu, Q. Guo, Enhanced activity of CuFe/SiO2 catalyst for CO hydrogenation to higher alcohols by pretreating the support with ammonia, J. Ind. Eng. Chem. 25 (2015) 338–343.
[38] M. Konsolakis, M. Sgourakis, S.A.C. Carabineiro, Surface and redox properties of cobalt–ceria binary oxides: on the effect of Co content and pretreatment conditions, Appl. Surf. Sci. 341 (2015) 48–54.
[39] N. Liu, Y.-x. Gao, W.-d. Wang, W.-x. Huang, Cu-Co composite oxides supported on multi-walled carbon nanotubes for catalytic removal of CO in a H2-rich stream, Chin. J. Chem. Phys. 27 (2014) 523–529.
[40] N.S. Gajbhiye, G. Balaji, S. Bhattacharyya, M. Ghafari, Mössbauer studies of nanosize CuFe2O4 particles, Hyperfine Interact. 156 (2004) 57–61.
[41] H. Yan, X.-T. Qin, Y. Yin, Y.-F. Teng, Z. Jin, C.-J. Jia, Promoted Cu-Fe3O4 catalysts for low-temperature water gas shift reaction: optimization of Cu content, Appl. Catal., B 226 (2018) 182–193.
[42] R. Huang, J. Xu, J. Wang, X. Sun, W. Qi, C. Liang, D.S. Su, Oxygen breaks into carbon nanotubes and abstracts hydrogen from propane, Carbon 96 (2016) 631–640.
[43] J.L. Figueiredo, M.F.R. Pereira, The role of surface chemistry in catalysis with carbons, Catal. Today 150 (2010) 2–7.
[44] K.V.R. Chary, K.K. Seela, G.V. Sagar, B. Sreedhar, Characterization and reactivity of niobia supported copper oxide catalysts, J. Phys. Chem. B 108 (2004) 658–663.
[45] S. Nishimura, A. Takagaki, K. Ebitani, Characterization, synthesis and catalysis of hydrotalcite-related materials for highly efficient materials transformations, Green Chem. 15 (2013) 2026–2042.
[46] M. Jabłońska, R. Palkovits, Copper based catalysts for the selective ammonia oxidation into nitrogen and water vapour—Recent trends and open challenges, Appl. Catal., B 181 (2016) 332–351.
[47] Z. Yuan, L. Wang, J. Wang, S. Xia, P. Chen, Z. Hou, X. Zheng, Hydrogenolysis of glycerol over homogenously dispersed copper on solid base catalysts, Appl. Catal., B 101 (2011) 431–440.
[48] H. Jin, R. You, S. Zhou, K. Ma, M. Meng, L. Zheng, J. Zhang, T. Hu, In-situ DRIFTS and XANES identification of copper species in the ternary composite oxide catalysts CuMnCeO during CO preferential oxidation, Int. J. Hydrogen Energy 40 (2015) 3919–3931.
[49] N. Liu, X. Chen, J. Zhang, J.W. Schwank, DRIFTS study of photo-assisted catalytic CO + NO redox reaction over CuO/CeO2-TiO2, Catal. Today 258 (Part 1) (2015) 139–147.
[50] A. Hornés, P. Bera, A.L. Cámara, D. Gamarra, G. Munuera, A. Martínez-Arias, CO-TPR-DRIFTS-MS in situ study of CuO/Ce1 − xTbxO2 − y (x = 0, 0.2 and 0.5) catalysts: support effects on redox properties and CO oxidation catalysis, J. Catal. 268 (2009) 367–375.
[51] M. Adamowska, A. Krztoń, M. Najbar, P. Da Costa, G. Djéga-Mariadassou, DRIFT study of the interaction of NO and O2 with the surface of Ce0.62Zr0.38O2 as deNOx catalyst, Catal. Today 137 (2008) 288–291.
[52] J. Ashok, S. Reema, C. Anjaneyulu, M. Subrahmanyam, A. Venugopal, Methane decomposition catalysts for CO x-free hydrogen production, Rev. Chem. Eng. 26 (2010) 29–39.
[53] N. Shah, D. Panjala, G.P. Huffman, Hydrogen production by catalytic decomposition of methane, Energ. Fuel. 15 (2001) 1528–1534.
[54] Y. Shen, A.C. Lua, Synthesis of Ni and Ni–Cu supported on carbon nanotubes for hydrogen and carbon production by catalytic decomposition of methane, Appl. Catal., B 164 (2015) 61–69.
[55] W. Shen, Y. Wang, X. Shi, N. Shah, F. Huggins, S. Bollineni, M. Seehra, G. Huffman, Catalytic nonoxidative dehydrogenation of ethane over Fe–Ni and Ni catalysts supported on Mg(Al)O to produce hydrogen and easily purified carbon nanotubes, Energ. Fuel. 21 (2007) 3520–3529.
[56] W. Shen, F.E. Huggins, N. Shah, G. Jacobs, Y. Wang, X. Shi, G.P. Huffman, Novel Fe–Ni nanoparticle catalyst for the production of CO- and CO2-free H2 and carbon nanotubes by dehydrogenation of methane, Appl. Catal., A 351 (2008) 102–110.
[57] J.F. Moulder, J. Chastain, Handbook of X-ray Photoelectron Spectroscopy: A Reference Book of Standard Spectra for Identification and Interpretation of XPS Data, Physical Electronics Division, Perkin-Elmer Corporation, 1992.
[58] Y. Song, X. Liu, L. Xiao, W. Wu, J. Zhang, X. Song, Pd-Promoter/MCM-41: a highly effective bifunctional catalyst for conversion of carbon dioxide, Catal. Lett. 145 (2015) 1272–1280.
[59] D. Briggs, C.D. Wanger, W.M. Riggs, L.E. Davis, J.F. Moulder, G.E. Muilenberg (Eds.), Handbook of X-Ray Photoelectron Spectroscopy, Perkin-Elmer Corp., Physical Electronics Division, Eden Prairie, Minnesota, USA, 1979190 pp. $195, Surf. Interface Anal., 3 1981 191-195.
[60] T.I.T. Okpalugo, P. Papakonstantinou, H. Murphy, J. McLaughlin, N.M.D. Brown, High resolution XPS characterization of chemical functionalised MWCNTs and SWCNTs, Carbon 43 (2005) 153–161.
[61] I. Nedkov, R.E. Vandenberghe, T. Marinova, P. Thailhades, T. Merodiiska, I. Avramova, Magnetic structure and collective Jahn–Teller distortions in nanostructured particles of CuFe2O4, Appl. Surf. Sci. 253 (2006) 2589–2596.
[62] A. Arango-Díaz, E. Moretti, A. Talon, L. Storaro, M. Lenarda, P. Núñez, J. Marrero-Jerez, J. Jiménez-Jiménez, A. Jiménez-López, E. Rodríguez-Castellón, Preferential CO oxidation (CO-PROX) catalyzed by CuO supported on nanocrystalline CeO2 prepared by a freeze-drying method, Appl. Catal., A 477 (2014) 54–63.
[63] L.E. Gómez, A.V. Boix, E.E. Miró, Co/ZrO2, Co/CeO2 and MnCoCe structured catalysts for COPrOx, Catal. Today 216 (2013) 246–253.
[64] P. Landon, J. Ferguson, B.E. Solsona, T. Garcia, S. Al-Sayari, A.F. Carley, A.A. Herzing, C.J. Kiely, M. Makkee, J.A. Moulijn, A. Overweg, S.E. Golunski, G.J. Hutchings, Selective oxidation of CO in the presence of H2, H2O and CO2 utilising Au/[small alpha]-Fe2O3 catalysts for use in fuel cells, J. Mater. Chem. 16 (2006) 199–208.
[65] Y. Liu, Q. Fu, M.F. Stephanopoulos, Preferential oxidation of CO in H2 over CuO-CeO2 catalysts, Catal. Today 93–95 (2004) 241–246.
[66] E.O. Jardim, S. Rico-Francés, F. Coloma, J.A. Anderson, E.V. Ramos-Fernandez, J. Silvestre-Albero, A. Sepúlveda-Escribano, Preferential oxidation of CO in excess of H2 on Pt/CeO2–Nb2O5 catalysts, Appl. Catal., A 492 (2015) 201–211.
[67] A. Manasilp, E. Gulari, Selective CO oxidation over Pt/alumina catalysts for fuel cell applications, Appl. Catal., B 37 (2002) 17–25.
[68] Y. Gao, K. Xie, W. Wang, S. Mi, N. Liu, G. Pan, W. Huang, Structural features and catalytic performance in CO preferential oxidation of CuO-CeO2 supported on multi-walled carbon nanotubes, Catal. Sci. Technol. 5 (2015) 1568–1579.
[69] L. Yu, Y. Liu, F. Yang, J. Evans, J.A. Rodriguez, P. Liu, CO oxidation on Gold-supported iron oxides: new insights into strong oxide–metal interactions, J. Phys. Chem. C 119 (2015) 16614–16622.
[70] L. Oar-Arteta, A.T. Aguayo, A. Remiro, J. Bilbao, A.G. Gayubo, Behavior of a CuFe2O4/γ-Al2O3 catalyst for the steam reforming of dimethyl ether in reaction-regeneration cycles, Ind. Eng. Chem. Res. 54 (2015) 11285–11294.
[71] S. Lu, C. Zhang, Y. Liu, Carbon nanotube supported Pt–Ni catalysts for preferential oxidation of CO in hydrogen-rich gases, Int. J. Hydrogen Energy 36 (2011) 1939–1948.
[72] E.O. Jardim, M. Gonçalves, S. Rico-Francés, A. Sepúlveda-Escribano, J. Silvestre-Albero, Superior performance of multi-wall carbon nanotubes as support of Pt-

based catalysts for the preferential CO oxidation: effect of ceria addition, Appl. Catal., B 113–114 (2012) 72–78.
[73] B. Li, C. Wang, G. Yi, H. Lin, Y. Yuan, Enhanced performance of Ru nanoparticles confined in carbon nanotubes for CO preferential oxidation in a H2-rich stream, Catal. Today 164 (2011) 74–79.
[74] H.-C. Wu, T.-C. Chen, J.H. Wu, C.-H. Chen, J.-F. Lee, C.-S. Chen, The effect of an Fe promoter on Cu/SiO2 catalysts for improving their catalytic activity and stability in the water-gas shift reaction, Catal. Sci. Tech. 6 (2016) 6087–6096.
[75] L. Dong, L. Liu, Y. Lv, J. Zhu, H. Wan, B. Liu, F. Gao, X. Wang, L. Dong, Y. Chen, Surface structure characteristics of CuO/Ti 0.5Sn 0.5O 2 and its activity for CO oxidation, J. Mol. Catal. A: Chem. 365 (2012) 87–94.